Dyes and Pigments 242 (2025) 112922

Contents lists available at ScienceDirect

Dyes and Pigments

journal homepage: www.elsevier.com/locate/dyepig

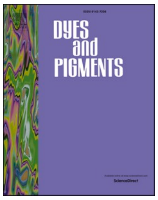

Polycyclic 1,2,5-chalcogenadiazole dyes: structural, optical, and redox properties in neutral and radical-ion states (chalcogen = S, Se)[☆]

Ekaterina A. Radiush [a], Vladislav M. Korshunov [b,d,*], Elena A. Chulanova [a,1], Lidia S. Konstantinova [c], Alexey I. Ferulev [d], Irina G. Irtegova [a], Inna K. Shundrina [a], Ekaterina A. Frank [a], Nikolay A. Semenov [a], Ilya V. Taidakov [b], Oleg A. Rakitin [c], Leonid A. Shundrin [a,**], Andrey V. Zibarev [a]

[a] *Vorozhtsov Institute of Organic Chemistry, Siberian Branch, Russian Academy of Sciences, 630090, Novosibirsk, Russia*
[b] *Lebedev Physical Institute, Russian Academy of Sciences, 119991, Moscow, Russia*
[c] *Zelinsky Institute of Organic Chemistry, Russian Academy of Sciences, 119991, Moscow, Russia*
[d] *Bauman Moscow State Technical University, 105005, Moscow, Russia*

ARTICLE INFO

Keywords:
1,2,5-Chalcogenadiazoles
Molecular structure
Optical properties
Redox activity
Radical ions

ABSTRACT

Neutral **M** and radical-ion $[\mathbf{M}]^{\cdot-}$ and $[\mathbf{M}]^{\cdot+}$ states of phenanthro- (**1**, **2**)/dibenzoquinoxalino- (**3**, **4**) fused 1,2,5-chalcogenadiazoles are studied; chalcogen = S (**1**, **3**), Se (**2**, **4**). Experimentally, **1**–**4** are characterized by simultaneous thermogravimetry – differential scanning calorimetry, spectroelectrochemistry and optical (UV–Vis–NIR/FL) spectroscopy, **2**–**4** by cyclic voltammetry (CV) for reduction and oxidation, and $[\mathbf{M}]^{\cdot-}$ by electron paramagnetic resonance ($[\mathbf{M}]^{\cdot+}$ were not detected). Compounds **3**, **4** and $[\mathbf{M}]^{\cdot-}$ (in the form of $[\mathrm{K(18\text{-}crown\text{-}6)}]^+$ salts; **M** = **1**, **3**) are characterized by X-ray diffraction (all are planar), and $[\mathbf{M}]^{\cdot-}$ (**M** = **1**–**4**) by UV–Vis–NIR. Theoretically, **M** and $[\mathbf{M}]^{\cdot-}$ (**M** = **1**–**4**) are specified by density functional theory (DFT) calculations. As compared with the archetypal 2,1,3-benzothiadiazole (**5**), in **1**–**4** the π-extension and replacement of S by Se jointly lead to increase of DFT adiabatic electron affinity (0.8 → 2.1 eV), decrease of the absolute values of CV potentials (−1.5 → −0.5 V), broadening and bathochromic shifts of UV–Vis (~310 → ~420 nm) and FL (~380 → ~470 nm) bands. DFT adiabatic ionization energy of **1**–**4** of ~7.9 eV is invariant to their structure (**5**: 8.7 eV). FL spectra of **1**–**4** exhibit small Stokes shifts; and those of **2** and **3**, vibronic structures. The estimated excited-state lifetime τ_1 is ~1 ns (ns) for **3** and **4**, and ~2 ns for **2**, while long-time component τ_2 is ~9 ns for **2** and ~7 ns for **3**. The findings suggest that **1**–**4** are promising organic π-dyes/non-fullerene electron acceptors for small-molecule optoelectronics.

1. Introduction

Tailor-made organic π-dyes exhibiting strong absorption and emission across ultraviolet–visible–near-infrared (UV–Vis–NIR) area are highly demanded by optoelectronics. Crystalline self-assembled small-molecule polycyclic (hetero) aromatics are increasingly promising due to efficient charge delocalization and transport in combination with high absorption and emission of light [1–3] (relevant literature is too abundant to be cites completely; here and below only selected references are given). Amongst numerous π-scaffolds involved in the field, especially exciting are fused 1,2,5-chalcogenadiazoles, *e. g.* benzo- (Scheme 1; E = S, Se, Te) and azabenzo-derivatives, which can be variously, and practically infinitely, functionalized including introduction of chirality, for specific fundamentals and/or applications [4–33]. These substances exhibit a unique combination of tunable physical and chemical properties encompassing:

[☆] Electronic supplementary information (ESI) available containing chemical names of the title compounds, XRD, UV–Vis and FL (embracing NIR), CV, SEC, EPR, and DFT data, together with additional discussion. CCDC 2338054–2338058. For ESI and crystallographic data in CIF or other electronic format see DOI: https://doi.org/10.1016/j.dyepig.2025.112922.

[*] Corresponding author. Lebedev Physical Institute, Russian Academy of Sciences, 119991, Moscow, Russia.

[**] Corresponding author. Vorozhtsov Institute of Organic Chemistry, Siberian Branch, Russian Academy of Sciences, 630090 Novosibirsk, Russia.

E-mail addresses: vladkorshunov@bk.ru (V.M. Korshunov), shundrin@nioch.nsc.ru (L.A. Shundrin).

[1] Current address: Department of Chemistry, University of Oxford, Oxford OX1 3QR, United Kingdom.

https://doi.org/10.1016/j.dyepig.2025.112922
Received 10 April 2025; Received in revised form 28 May 2025; Accepted 28 May 2025

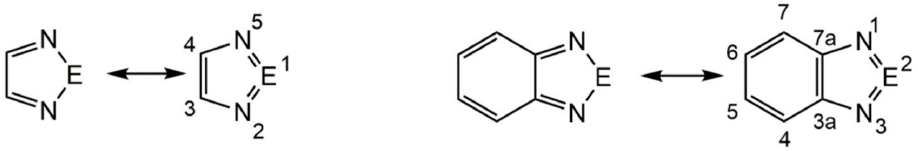

Scheme 1. 6π-Electron 1,2,5-chalcogenadiazoles and their 10π-electron benzo-fused derivatives, *i.e.*, 2,1,3-benzochalcogenadiazoles, together with atom numberings; E = S, Se and Te. Compounds are represented by the resonance superposition of quinoid and benzoid forms, whose ratio depends on the nature of the E atoms [35]; throughout the article, only the benzoid form is used to avoid the superpositions.

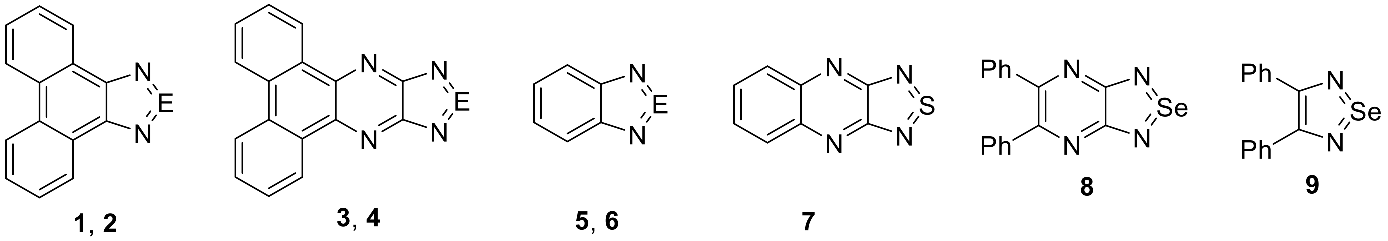

Scheme 2. Compounds **1**–**9**; E = S (**1**, **3**, **5**, **7**), Se (**2**, **4**, **6**, **8**, **9**).

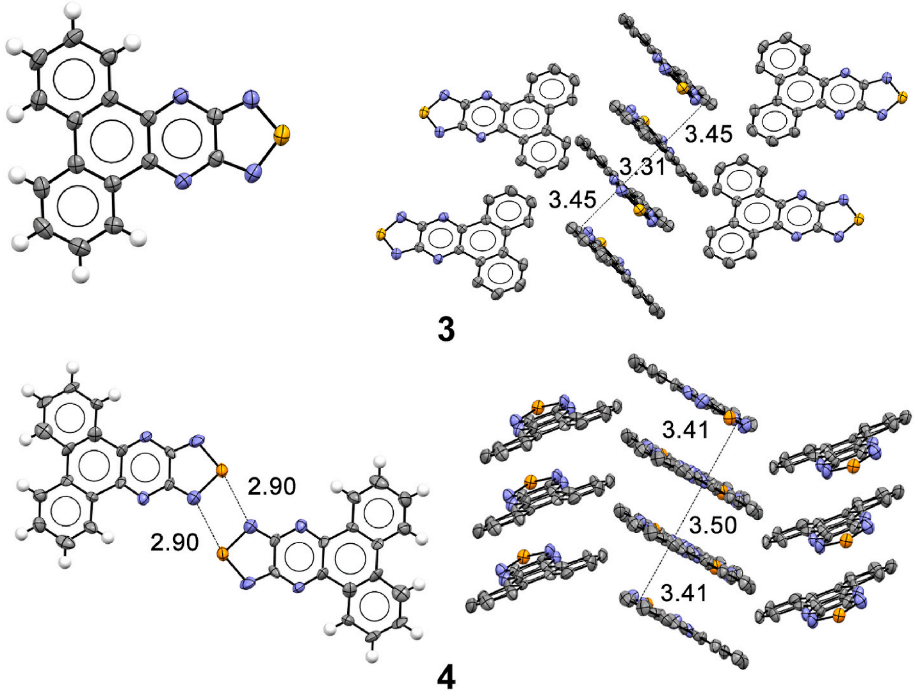

Fig. 1. XRD molecular structures and fragments of crystal structure of **3** (CCDC 2338054) and **4** (CCDC 2338055) exhibiting shortened intermolecular π-contacts, and **4** also [Se···N]$_2$ supramolecular synthon/*ChB* (dotted lines). Color code: C grey, H light grey, N blue, S (**3**)/Se (**4**) orange. For **1** [12] and **2** [39], see CCDC 783888 and 2034286, respectively. (For interpretation of the references to colour in this figure legend, the reader is referred to the Web version of this article.)

High thermal stability associated with their heteroaromaticity [34,35]; Structural diversity/capacity for π-extension spreading from the archetypes to variously fused polycyclics [11,28–33,36–43]; Lewis ambiphilicity [44] embracing self-assembly via tunable chalcogen bonding (*ChB*) [45,46] and some other secondary bonding interactions (SBIs) [47–60]; Positive first adiabatic electron affinity (aEA$_1$) manifesting in low-potential-electrochemical and chemical reduction into thermodynamically-attractive radical anions (RAs) [5,6,12,61–66] (and fused 1,2,5-thia/selenadiazoles belong to the most-efficient non-fullerene electron acceptors used in organic optoelectronics [67–71]); Single-component chromophoric/fluorophoric performance including nonlinear, chiroptical and aggregation-induced, as well as electroluminescence [12–14,16,17,19–22,72–89].

The discussed properties strongly depend on the nature/polarizability of chalcogen atoms, π-extension and substitution pattern and, therefore, can be tuned [4,7,28,29,36,61,63,70,73,74,88–93]. The best studied are S derivatives; Se and Te ones attract steadily growing attention [8,9,43,60,61,94,95] motivated in part by stronger spin-orbit coupling (SOC) [96,97] inherent in heavier chalcogen atoms and promising for organic optoelectronics [98]. Alongside, fused 1,2,5-chalcogenadiazoles are involved in crystal engineering [38,39,42,47,99–102], electrocatalysis [103], chemosensorics [14,46,104,105], and bioimaging [30,31,73,74,76]; and their RAs (chalcogen = S) are suggested for energy storage with FL-enabled self-reporting nonaqueous redox flow batteries where they are charge carriers [7,106–108].

The π-extension via annulation is an effective tool to increase aEA$_1$

Table 1
(U)B3LYP/def2-tzvp-calculated αEA_1 and αIE_1 of compounds **1**–**8**, together with negatives of the frontier MOs energies and ΔE of **1**–**4** (eV).[a]

Compound	1	2	3	4	**5**	**6**	**7**	8
αEA_1[b]	0.82	1.00	2.02	2.13	0.82	1.02	2.11	1.90
αIE_1	7.97	7.89	7.98	7.92	8.74	8.53	8.62	7.90

[a] αEA_1 and αIE_1 are taken as the energy difference of fully optimized neutral and corresponding radical-ion states. For **1**–**4**, negatives of one-electron energies of the frontier MOs (HOMO/LUMO) and their energy gap (ΔE) are (eV): **1**: 5.68/2.94 (2.74); **2**: 5.61/3.06 (2.55); **3**: 6.59/3.67 (2.92); **4**: 6.56/3.74 (2.82).

[b] For comparison, measured EA_1 is 2.67 eV for C_{60} fullerene [132], 5.50–5.87 eV for trimethylenecyclopropanes bearing electron-accepting groups, and 5.24 eV for tetrafluorinated 7,7,8,8-tetracyanoquinodimethane [133]; for some relevant fused 1,2,5-chalcogenadiazoles, see Ref. [63].

and decrease π-excitation energies. An annulation mode is important as evidenced by polycyclic aromatic hydrocarbons where transition from naphthalene to isomeric linear anthracene and angular phenanthrene changes αEA_1 differently [109,110]. For further work with exceptionally wide variety of 1,2,5-chalcogenadiazoles' structures and properties, especially promising are less-studied highly-annulated/π-extended, but still small-molecule, derivatives such as **1**–**4** [12,38,111] (Scheme 2) combining both linear and angular annulation. Of them, **1** [112,113] and **4** [114] are already involved in materials science. At the molecular level, however, stereoelectronic properties of **1**–**4** and, especially, their single-electron reduced/oxidized states, *i.e.*, radical ions $[\mathbf{M}]^{\cdot-}$ and $[\mathbf{M}]^{\cdot+}$ ($\mathbf{M} = \mathbf{1}$–$\mathbf{4}$), are not comprehensively characterized, with partial exceptions for **1** [12] and **2** [39]. Here we report on the thermal, structural, optical and redox properties of **1**–**4** and their radical ions. Compounds **1**–**4** are characterized by TG-DSC, CV and SEC; **3** and **4**, by XRD; and $[\mathbf{M}]^{\cdot-}$ ($\mathbf{M} = \mathbf{1}$–$\mathbf{4}$), by EPR and UV–Vis–NIR ($[\mathbf{M}]^{\cdot+}$ are not observed). Theoretically, **M** and $[\mathbf{M}]^{\cdot-}$ ($\mathbf{M} = \mathbf{1}$–$\mathbf{4}$) are specified by DFT

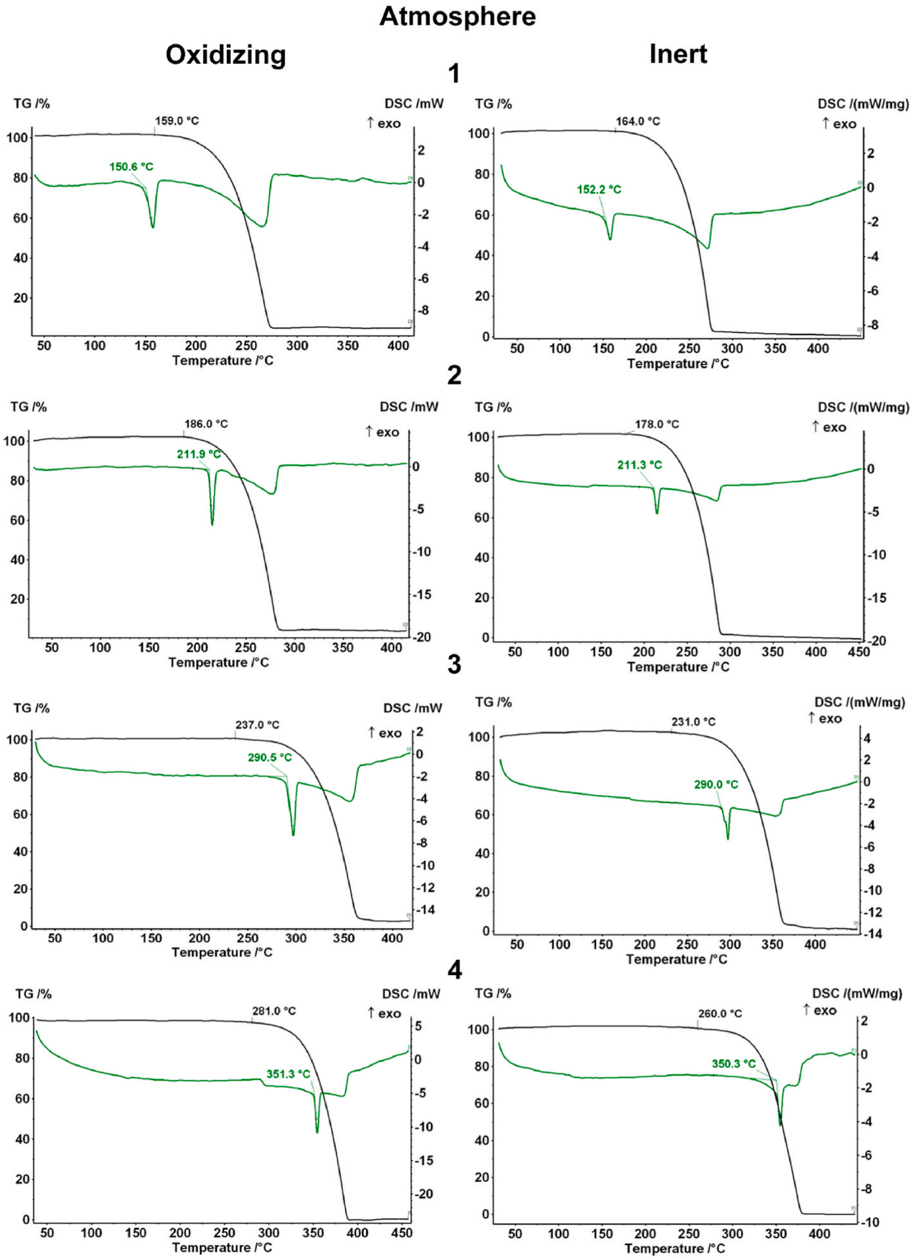

Fig. 2. Thermal stability of **1**–**4** in inert (He) and oxidizing (He/O_2, %: 80/20) atmospheres. Color code: TG black, DSC green. (For interpretation of the references to colour in this figure legend, the reader is referred to the Web version of this article.)

Table 2
Photophysical properties of compounds **1**–**6** in MeCN.

Compound	Wavelength, nm		Lifetimes τ_1/τ_2, ns
	absorption λ_{max}/λ_{on}[a] measured (log ε)/TD-DFT calculated	emission λ_{max}/ excitation λ_{ex}[b]	
1	344/355 (4.2), shoulder 360–480/390	403/310	–
2	366/374 (4.2)/398	426/346	1.8/9.0
3	399/447 (4.4), shoulder 410–420/402	413, 436/310	1.3/7.0
4[c,d]	413/457 (4.5), shoulder 425–430/428	465/405	1.4/–
5	308 (3.9)/–	383/309	–
6	332 (4.2)/–	400/356	–

[a] λ_{max} and λ_{on} are the maximum and red-side onset of the longest-wavelength absorption band, respectively.
[b] Excitation wavelengths.
[c] For ~30-nm thin-film absorption and emission spectra, see Ref. [114].
[d] For ~30-nm thin-film, poorly resolved structure of emission band is observed; $\tau_1 < 0.6$ ns and $\tau_2 > 1.5$ ns [114].

and TD-DFT calculations. As reference compounds, S/Se derivatives **5**–**9** (Scheme 2) are used; Te analogs are not involved due to low solubility in common organic solvents caused by strong Te···N SBIs/*ChB* [49–51,57,115,116]. RA salts are prepared by chemical reduction of **1**–**4**, **8**, **9**; and [K(18-crown-6)]$^+$[**M**]$^{\cdot-}$ (**M** = **1**, **3**, **8**) are characterized by XRD and UV–Vis–NIR to support SEC/EPR observations.

Critical parameter of optoelectronic materials is the energy gap ΔE between the highest occupied and the lowest unoccupied electronic levels. It can be evaluated experimentally and theoretically. Different approaches lead to conceptually different energy gaps, which should be clearly distinguished [117]. In this work, a combination of experimental electrochemical and optical data was used.

2. Experimental

2.1. General

Compounds **1** [12], **2** [39], **3** [111], **4**, **8**, **9** [38], and KC$_8$ [118] were prepared by known methods; cyclic polyether 18-crown-6 was received from Aldrich. Solvents were dried by common drying agents. Syntheses of RA salts were carried out in the argon glovebox and/or with Schlenk technique. Elemental analyses for C, H, and N were carried out with CHNS-Analyzer Euro EA 3000.

2.2. Synthesis

[K(18-crown-6)] [1]$^{\cdot-}$**.** A mixture of 0.003 g (0.08 mmol) of elemental potassium, 0.022 g (0.08 mmol) of 18-crown-6 and 0.020 g (0.08 mmol) of **1** in 3 ml of thf was stirred overnight, and then slowly evaporated. Salt [K(18-crown-6)][**1**]$^{\cdot-}$ was obtained in the form of brown crystals suitable for XRD.

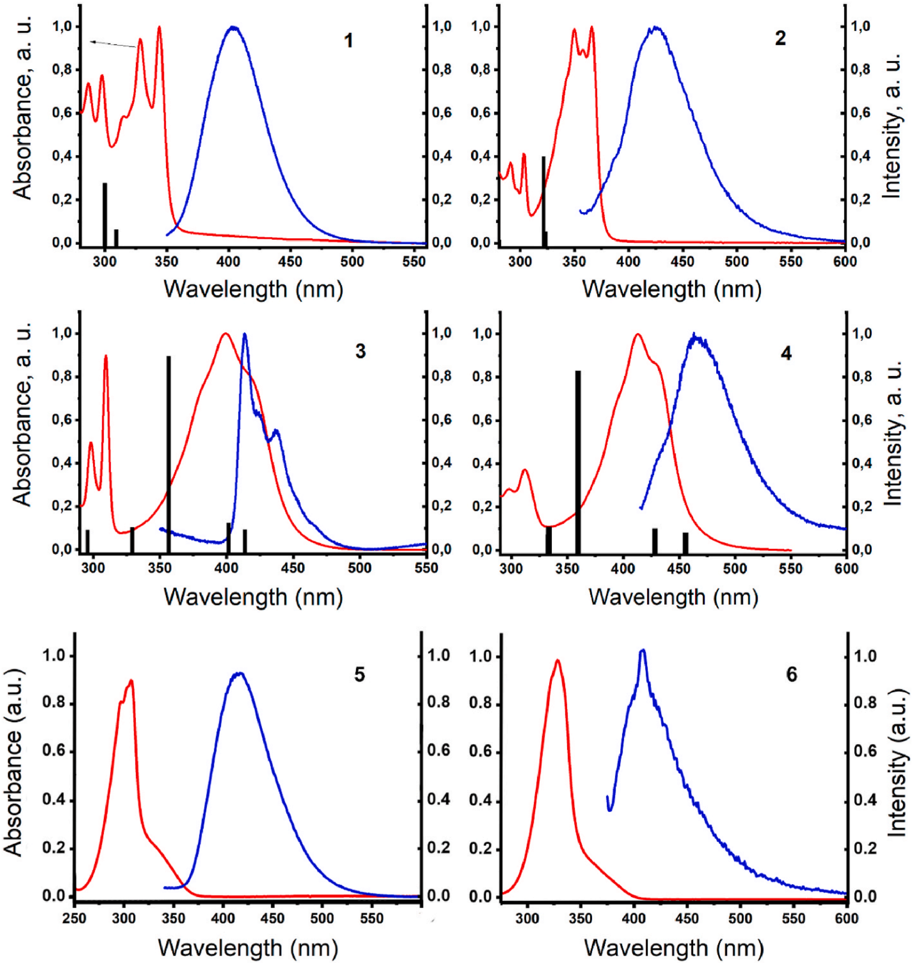

Fig. 3. Absorption (red) and emission (blue) spectra of **1**–**6** in MeCN, together with positions and relative intensities of electronic transitions in the absorption spectra (black bars) calculated by TD-DFT at the BLYP/def2-tzvp level of theory for **1** and **2**, and the B3LYP/def2-tzvp level for **3** and **4**. (For interpretation of the references to colour in this figure legend, the reader is referred to the Web version of this article.)

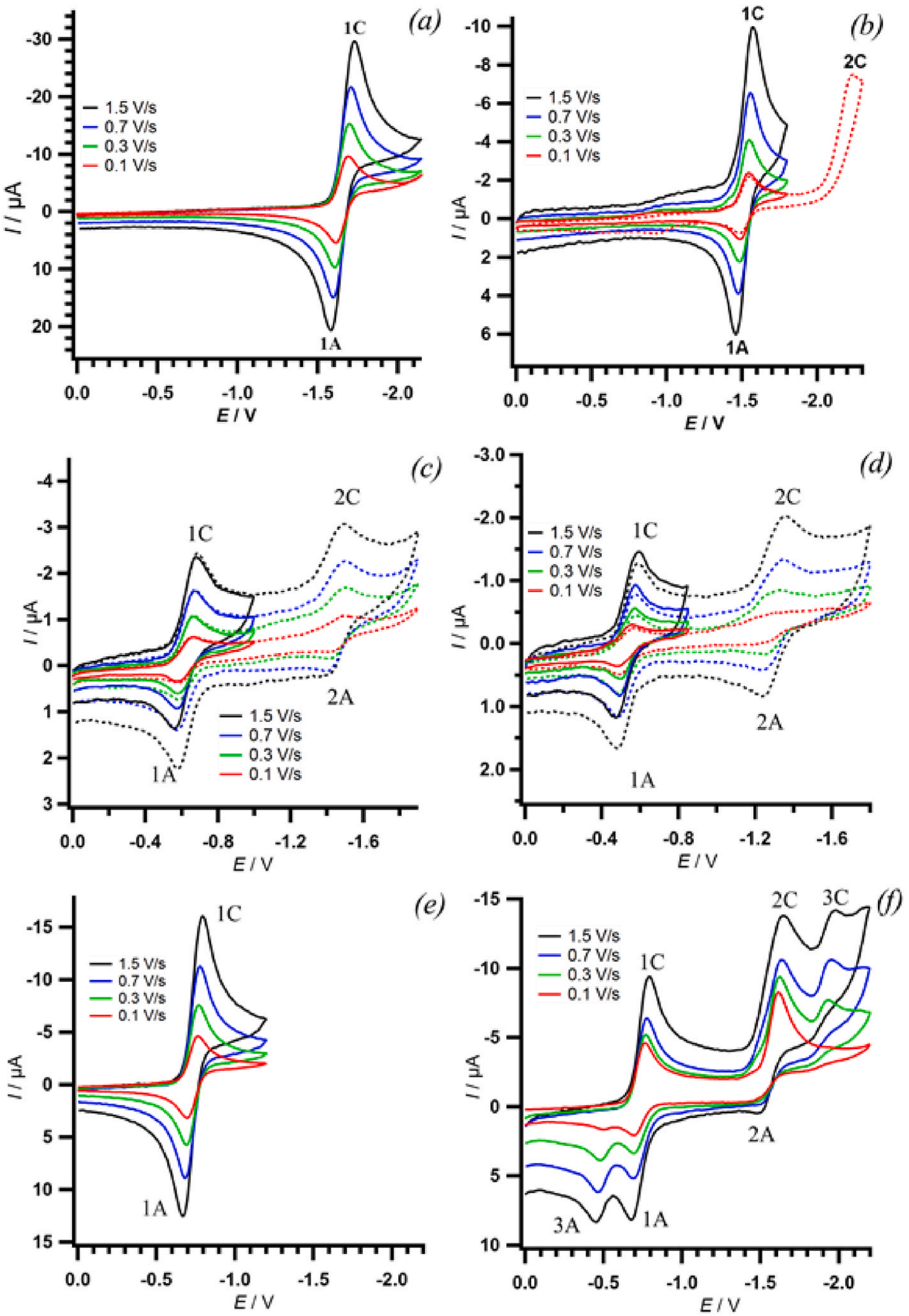

Fig. 4. CVs of compounds in MeCN at various potential sweep rates indicated by colour: (*a*) **1**, (*b*) **2**, (*c*) **3**, (*d*) **4**, (*e*) **8** (the first wave), and (*f*) **8** (full sweep). (For interpretation of the references to colour in this figure legend, the reader is referred to the Web version of this article.)

[K(18-crown-6)] [**3**]$^{-}$**.** A mixture of 0.008 g (0.05 mmol) of potassium thiophenolate, 0.014 g (0.05 mmol) of 18-crown-6 and 0.015 g (0.05 mmol) of **3** in 3 ml of MeCN was stirred overnight, and then slowly evaporated. Salt [K(18-crown-6)][**3**]$^{-}$ was obtained in the form of brown crystals suitable for XRD.

[K(18-crown-6)] [**8**]$^{\bullet-}$**.** A mixture of 0.020 g (0.15 mmol) of KC_8, 0.039 g (0.15 mmol) of 18-crown-6 and 0.050 g (0.15 mmol) of **8** in 10 ml of thf was stirred overnight. Reaction mixture was filtered, and the filtrate was mixed with 10 ml of pentane, stirred for 15 min, and the precipitate was filtered off and dried under vacuum. Salt [K(18-crown-6)][**8**]$^{\bullet-}$ was obtained in the form of black powder (0.057 g, 60 %). Elemental analysis, %, found/calculated for $C_{28}H_{34}KN_4O_6Se$: C 52.02/C 52.43, H 4.89/5.35, N 8.83/8.75. Single crystals, suitable for XRD were obtained via slow evaporation of toluene solution.

2.3. X-ray diffraction

The X-ray diffraction (XRD) experiments (ESI) were performed with a Bruker Kappa Apex II CCD diffractometer by using a graphite-monochromated MoKα irradiation. The structures were solved by the direct method using the *SHELX-97* program [119] and refined by full-matrix least-squares method against all F^2 in anisotropic approximation using the *OLEX2* program [120]. The H atoms positions were calculated with the riding model. Absorption corrections were applied using the empirical multiscan method with the *SADABS* programs [121]. The obtained crystal structures were analyzed for shortened contacts

Table 3
Peak [a] and half-wave potentials (V) of compounds **M** in solvents S, diffusion coefficients [b] (D × 10^{-5}, $cm^2 \cdot s^{-1}$) in MeCN, negatives of the frontier MOs (HOMO/LUMO) energies and the energy gap ΔE between the highest occupied and the lowest unoccupied electronic levels (eV) estimated from CV and optical data.[c,d]

M	S	D	E_p^{1C}	E_p^{1A}	$E^1_{1/2}$	E_p^{2C}	E_p^{2A}	$E^2_{1/2}$	HOMO/LUMO	ΔE
1	MeCN	1.0	−1.68	−1.62	−1.65	–	–	–	6.21/2.72	3.49
2	MeCN	0.94	−1.54	−1.49	−1.52	−2.23	–	–	6.16/2.85	3.31
	CH_2Cl_2	–	−1.51	−1.38	−1.45	–	–	–	–	–
3	MeCN	0.91	−0.66	−0.60	−0.63	−1.49	−1.42	−1.46	6.51/3.74	2.77
	CH_2Cl_2	–	−0.59	−0.49	−0.54	−1.38	−1.29	−1.34	–	–
4	MeCN	0.43	−0.55	−0.49	−0.52	−1.33	−1.25	−1.29	6.56/3.85	2.71
	CH_2Cl_2	–	−0.48	−0.41	−0.45	−1.19	−1.12	−1.16	–	–
8	MeCN	0.8	−0.76	−0.70	−0.73	−1.62	−1.52	−1.57	6.51/3.64	2.87

[a] The E_p potentials are measured at the 0.1 V s^{-1} sweep rate and quoted with the reference to SCE.

[b] Determined from the Randles-Ševčik and Cottrell analyses [123] (ESI).

[c] The LUMOs energies are calculated from the $E^1_{1/2}$ values (MeCN) with ferrocene (4.8 eV) as the reference compound; the HOMOs energies are calculated as the difference between those of the LUMOs obtained with CV data and optical gap 1240/λ_{on} (MeCN; Table 2). For 1–4, cf. DFT-calculated energies and ΔE of the frontier MOs (Table 1).

[d] The DFT-calculated αEA_1 (Table 1) correlates with the $E^1_{1/2}$ measured in MeCN (ESI); E_p^{1C} of 5 and 6 is ~ −1.5 and −1.3 V vs. SCE, respectively [63].

between non-bonded atoms using the *Mercury* program [122]. CCDC 2338054 (**3**), 2338055 (**4**), 2338056 ($[K(18\text{-crown-6})]^+[\mathbf{1}]^{\cdot-}$), 2338057 ($[K(18\text{-crown-6})]^+[\mathbf{3}]^{\cdot-}$), and 2338058 ($[K(18\text{-crown-6})]^+[\mathbf{8}]^{\cdot-}$) contain the supplementary crystallographic data for this paper. The data can be obtained free of charge via www.ccdc.cam.ac.uk/data_request/cif, or by emailing data_request@ccdc.cam.ac.uk, or by contacting The Cambridge Crystallographic Data Centre, 12 Union Road, Cambridge CB2 1EZ, UK; fax: +44 1223 336033.

2.4. Simultaneous thermogravimetry – differential scanning calorimetry

The simultaneous thermogravimetry – differential scanning calorimetry (TG-DSC) measurements were performed in inert (He) and oxidizing (He/O_2, %: 80/20) atmospheres with a Netzsch STA 409 instrument equipped with platinum pan at a heating rate of 10 °C min^{-1}. Temperature and heat flow calibration was performed according to ISO 11357-1 standard by the temperatures and enthalpies of phase transitions of standard substances from the Netzsch calibration set (C_6H_5COOH (99.5 %), $RbNO_3$ (99.99 %), In (99.99 %), Sn (99.99 %), Bi (99.9995 %) and Zn (99.999 %). The obtained data were processed using *Netzsch Proteus Thermal Analysis* software.

2.5. Electrochemistry

2.5.1. Cyclic voltammetry

Cyclic voltammetry (CV) measurements on **1**–**4** and **8** were performed in MeCN and CH_2Cl_2 at 295 K in an argon atmosphere using a standard electrochemical glass cell with a solution volume of 5 mL connected to a PG 310 USB potentiostat (HEKA Elektronik, Germany) with a three-electrode circuit. A stationary Pt disc electrode (electrode area $A = 0.0122$ cm^2) calibrated with Fc/Fc^+ system as a standard was used as a working electrode; and a Pt helix, as an auxiliary electrode. Peak potentials were quoted with a reference to a saturated calomel electrode (SCE) connected to the cell using a bridge with 0.1 M of supporting electrolyte in MeCN/CH_2Cl_2. A 0.1 M solution of $[Et_4N][ClO_4]$ in MeCN/CH_2Cl_2 was used as a supporting electrolyte. All CV curves were measured using a triangular potential sweep within the potential sweep rates 0.1–1.5 V s^{-1}. The dependences of the first reduction peak current on potential sweep rate were analyzed with Randles-Ševčik equation [123] using *Matlab R2018b* software.

2.5.2. Cottrell analysis

Cottrell curves (CCs) [123] for **1**–**4** and **8** were measured in MeCN under the same experimental conditions as in the CV experiments. The initial potential was held at 0.0 V (vs. SCE) for 10 s, and then pulsed to the corresponding values (ESI). The duration of Cottrell measurements was 15 s. The experiments were carried out in two steps at the same potentials. The first step included a blank experiment without a depolarizer. The second step was carried out after adding the depolarizer. The resulting CCs were obtained as the difference between the second step curves and the blank curves, and analyzed with the *Matlab R2018b* software.

2.6. EPR spectroscopy

Electron paramagnetic resonance (EPR) spectra of $[\mathbf{M}]^{\cdot-}$ (**M** = **1**–**4**, **8**) were measured with an ELEXSYS E−540 spectrometer (X-band, MW frequency ~9.87 GHz, MW power 20 mW, modulation frequency 100 kHz, and modulation amplitude 0.007 mT) equipped with a high-Q cylindrical resonator ER4119HS. For the measurements, potentiostatic ECR of **M** (~1 mM in a dry MeCN (**1**–**4**, **8**) and CH_2Cl_2 (**2**–**4**) with 0.1 M $[Et_4N][ClO_4]$ as a supporting electrolyte) at the potential of the first cathode peak was carried out at 295 K under anaerobic conditions. Potentiostatic electrolysis was performed in an electrochemical cell for EPR measurements equipped with Pt working electrode with an Ellins P-20X potentiostat (Russia). Simulation of the experimental EPR spectra was accomplished with the *Winsim 2002* program [124]. The *Simplex* algorithm was used for optimization of hfc constants *a* and linewidths. The hfc constants $a^1H < 0.004$ mT, which are not exhibited in the spectra, were obtained by simulation.

2.7. Spectroelectrochemistry

Spectroelectrochemical (SEC) studies on **M** (M = **1**–**4**, **8**) were performed at 295 K in MeCN. The concentrations of **M** were optimized based on their solubility in MeCN. A CS9330 SEC cell (PR China) equipped with a Pt mesh working electrode was used; all cell manipulations were performed in a glovebox. An Ag/AgCl pseudo-reference electrode was used as a standard, and a Pt wire as a counter electrode. The cell was connected to a PG 310 USB potentiostat (HEKA Elektronik, Germany) with a three-electrode circuit and simultaneously to an Avantes AvaSpec-ULS2048CL-EVO UV–Vis–NIR spectrophotometer via a fiber-optical line. The UV–Vis–NIR spectra of the reduced solutions were recorded in a normal D(λ) and differential D(λ) − $D_{blank}(\lambda)$ forms, where D(λ) is the optical absorption spectrum recorded during electrochemical reduction (ECR), and $D_{blank}(\lambda)$ is the spectrum of **M** in MeCN recorded before the ECR. Cyclic electrolysis was performed in the potential sweep range covering the first one-electron reversible stage of the ECR with a potential sweep rate 5 mV s^{-1}. The effective volume of the cathode part of the SEC cell was $V = 6.3 \cdot 10^{-4}$ dm^3 as estimated by comparison of SEC and optically transparent electrode (OTE) measurements on **8** (ESI). The integration of macroelectrolysis time traces *I*(*t*) was performed using the *PotMaster* software (HEKA). The UV–Vis–NIR spectra of $[\mathbf{M}]^{\cdot-}$ were normalized with the *Matlab R2018b* program. Final

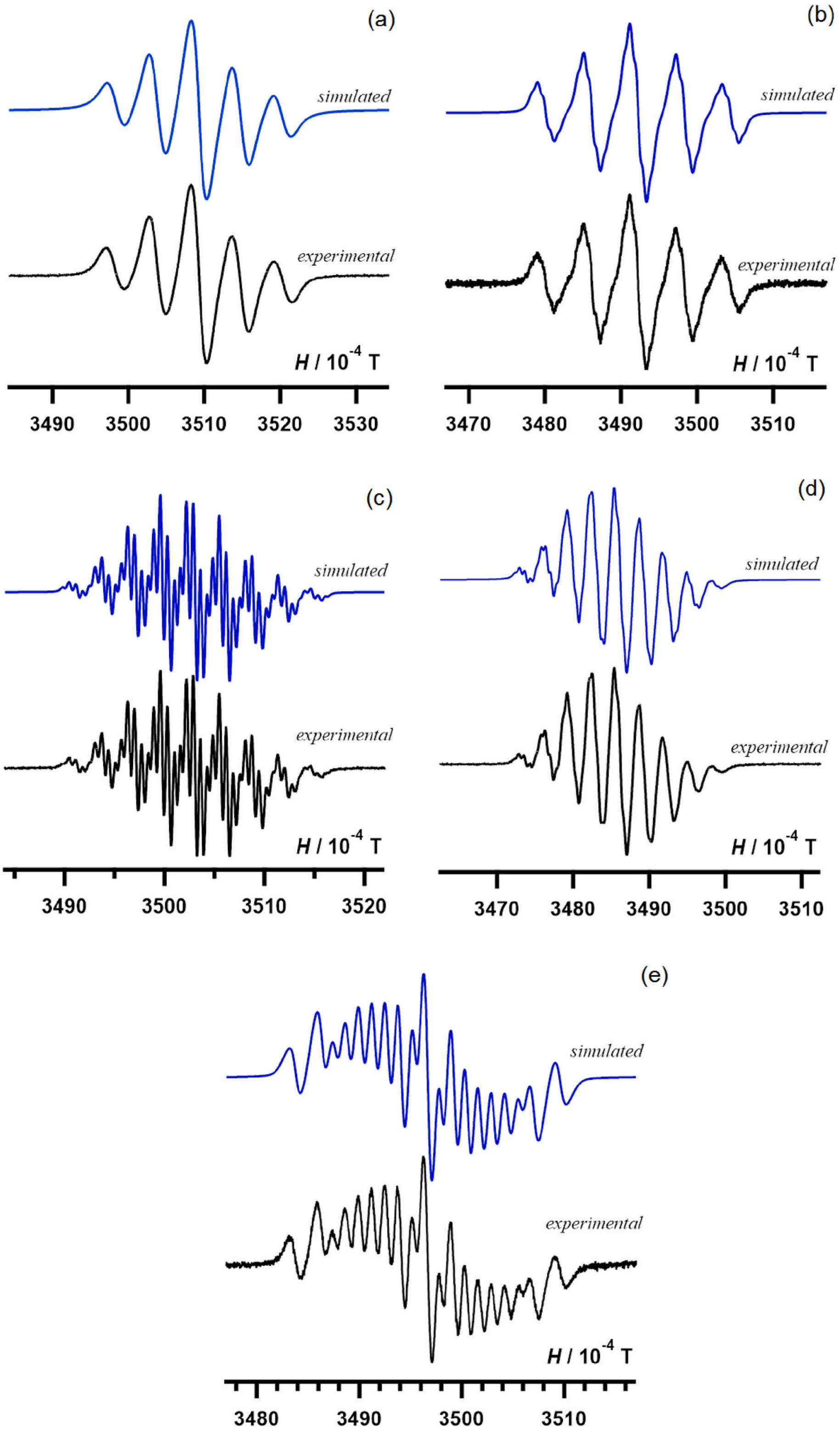

Fig. 5. EPR spectra at 295 K of (*a*) [**1**]$^{\cdot-}$ (MeCN), (*b*) [**2**]$^{\cdot-}$ (MeCN), (*c*) [**3**]$^{\cdot-}$ (CH_2Cl_2), (*d*) [**4**]$^{\cdot-}$ ($Me_2S{=}O$), and (*e*) [**8**]$^{\cdot-}$ (MeCN; for CV and EPR of [**8**]$^{\cdot-}$, see also [38]) obtained by potentiostatic electrolysis at the potentials of the first ECR peak. For hfc constants, see Table 4.

data analysis was performed using the *Igor PRO 8.0* software (Wavemetrics).

2.8. Photophysics

Electronic absorption (UV–Vis) spectra were collected using JASCO V-770 UV–Vis–NIR spectrophotometer. All the measurements were performed for solutions in quartz cells with a 1 cm pathlength. Photoluminescence spectra were measured using Horiba Jobin-Yvon Fluorolog QM-75-22-C spectrofluorimeter with a use of 75 W xenon arc lamp (PowerArc, HORIBA, Kyoto, Japan). A Hamamatsu R13456 (Hamamatsu Photonics, Hamamatsu, Japan) cooled photomultiplier tube

Table 4
Experimental and B3LYP/6-31g(*d*)-calculated hfc constants (G) in EPR spectra of $[\mathbf{M}]^{\cdot-}$ ($\mathbf{M} = \mathbf{1}$–$\mathbf{4}$, $\mathbf{8}$) obtained by potentiostatic electrolysis in different solvents at the potential of the first cathode peak.

$[\mathrm{M}]^{\cdot-}$	Solvent	Hfc constants	
		EPR	B3LYP
$[\mathbf{1}]^{\cdot-}$ [a]	MeCN	5.45 (2 N), 0.71 (2H), 0.37 (2H), 0.18 (2H)	5.53 ($2N_{diazole}$), −1.20 (H), −0.77 (H), 0.27 (H), 0.02 (H)
$[\mathbf{2}]^{\cdot-}$ [a]	MeCN	6.07 (2 N), 0.96 (2H), 0.64 (2H), 0.24 (2H)	5.65 ($2N_{diazole}$), −1.19 (H), −0.50 (H), 0.31 (H), −0.18 (H)
$[\mathbf{3}]^{\cdot-}$	CH_2Cl_2	3.30 (2 N), 2.57 (2 N), 0.76 (2H), 0.55 (2H), 0.16[a] (2H), 0.11[a] (2H)	3.72 ($2N_{pyrazine}$), 2.94 ($2N_{diazole}$), −0.80 (H), −0.50 (H), 0.26 (H), 0.000 (H)
$[\mathbf{4}]^{\cdot-}$	DMF	3.33 (2 N), 2.86 (2 N), 0.74 (2H), 0.59 (2H), 0.08[a] (2H), 0.05[a] (2H)	3.42 ($2N_{pyrazine}$), 3.09 ($2N_{diazole}$), −0.80 (H), −0.51 (H), 0.26 (H), 0.01 (H)
$[\mathbf{8}]^{\cdot-}$ [a]	MeCN	3.88 (2 N), 2.57 (2 N)	3.58 ($2N_{diazole}$), 3.20 ($2N_{pyrazine}$), −0.44 (H), −0.40 (H), −0.28 (H), 0.21 (H), 0.11 (H)

[a] The a^1H are smaller than EPR linewidths and were obtained by simulation only approximately.

sensitive in UV–Vis–NIR region (200–950 nm) was used as the detector. Photoluminescence decays (ESI) were collected by Time-correlated single photon counting (TCSPC) method using the same spectrofluorimeter. The setup included PicoQuant LDH-P-C-375B and LDH-P-C-405 (PicoQuant, Berlin, Germany) laser diode heads as a pulsed excitation source emitting at 376 nm and 405 nm with a repetition rate 1 MHz and pulse duration FWHM of 40 ps. Corresponding instrument response functions were taken into account for all optical measurements. The experiments were conducted in air at atmospheric pressure and room temperature. No tendency for the compounds to degradation of optical properties was observed during the measurements.

2.9. Quantum chemical calculations

Density functional theory (DFT) calculations of the first adiabatic electron affinity and ionization energy ($a\mathrm{EA}_1$ and $a\mathrm{IE}_1$, respectively), spin densities and Mulliken atomic charges (ESI) of **M**, $[\mathbf{M}]^{\cdot-}$ and $[\mathbf{M}]^{\cdot+}$ (M = **1**–**4**) were performed at the (U)B3LYP/def2-tzvp level of theory with full optimization using the *Gaussian09* suite of programs [125]. Time-dependent density functional theory (TD-DFT) [126] calculations were performed using BLYP/and B3LYP/def2-tzvp levels of theory with D3 version of Grimme's dispersion. The hfc constants were calculated at the (U)B3LYP/6-31g(d) level of theory.

3. Results and discussion

According to XRD (Fig. 1; ESI), molecules of **1**–**4** are planar, bond distances and bond angles are typical [127]. The crystal structures of **1** [12], **2** [39], and **4** (Fig. 1) exhibit typical S···N *ChBs* of 3.09 Å (**1**), or Se···N *ChBs* of 2.37–2.91 and 2.90 Å (**2**, **4**, respectively), forming $[\mathrm{E}\cdots\mathrm{N}]_2$ rhombic σ-dimers normal for solid 1,2,5-selenadiazoles [49,59,60,62,101,102,116,128]. In contrast, the crystal structure of **3** (Fig. 1) does not feature S···N *ChBs* forming lateral σ-dimers. Generally, the energy of E···N interactions (E = S, Se, Te) strongly depends on the nature of E and increases in the order S < Se < Te [51,57,129]. All **1**–**4** manifest favorable for charge transport shortened π-contacts/π-stacking with interplanar separations of 3.31–3.47 Å for **1** [12] and **3**, and 3.41–3.50 Å for **2** [39] and **4**, which are normal of (het) areno-fused 1,2,5-chalcogenadiazoles (chalcogen = S, Se) [102,130]. The sum of van der Waals (VdW) radii of S and N atoms is 3.55 Å; and Se and N atoms, 3.48 Å [131].

The DFT-calculated $a\mathrm{EA}_1$ of **1**–**4** varies on a broad scale from 0.82 to 2.13 eV; and the first adiabatic ionization energy ($a\mathrm{IE}_1$), on much narrow one from 7.89 to 7.98 eV (Table 1). Expansion of the conjugated π-system is expected to increase $a\mathrm{EA}_1$ [59,61,109,110], however, **1** and **2** exhibit virtually the same $a\mathrm{EA}_1$ as the archetypal **5** and **6**, respectively; whereas **3** and **4** have ~1 eV higher $a\mathrm{EA}_1$ (Table 1), which could be attributed to either the extension of a π-system or/and electron-accepting effect of pyrazine N atoms. However, if **7** is taken a parent compound for **3**, the extension of a π-system decreases $a\mathrm{EA}_1$ value by ~0.1 eV. The expanding of the conjugation on passing from **8** to **4** provides only ~0.2 eV increase in $a\mathrm{EA}_1$. Overall, it is seen that π-extension has its limitation as an instrument for the tuning of $a\mathrm{EA}_1$ values of polycyclic 1,2,5-chalcogenadiazoles. The calculated values are below EA_1 of C_{60} fullerene [132] (Table 1). It is important that for optoelectronics/photovoltaics applications of fullerene acceptors namely reduced EA_1 is required for better matching energy levels of donors [133] and the same can be expected for non-fullerene acceptors. For **1**–**4**, $a\mathrm{IE}_1$ of 1–2 eV, well-correlating with the first electrochemical reduction potential (see below and in ESI), suggests a challenging electron injection from standard electrode. The energy gap ΔE between the frontier MOs varies between ~2.6 (**2**) and ~2.9 (**3**) eV (Table 1); these values are, obviously, different [117] from those obtained experimentally (below).

Compounds **1**–**4** are thermally-stable in both inert and air-like oxidizing atmospheres, and volatile at normal pressure. The atmosphere slightly affects their melting temperatures of ~150 (**1**), 210 (**2**), 290 (**3**), and 350 (**4**) °C; as well as onset temperatures of mass loss (T_o) of ~160 (**1**, vaporization from melt), 180–185 (**2**, sublimation), and 230–235 (**3**, sublimation) °C. Compound **4** is exception with T_o ~260 (sublimation) under inert conditions, and ~280 °C (oxidation, sublimation) under oxidizing conditions (Fig. 2).

Similar to compounds **5**, **6**, and their derivatives [134–140], compounds **1**–**4** exhibit absorption in the visible spectral range. Their absorption spectra comprise multiple intense bands within the 280–320 nm region, attributed to π→π* electronic transitions, along with additional absorption bands located in the long-wavelength region. The latter bands demonstrate higher absorbance ($\log \varepsilon \sim 4.2$–$4.5$) compared to those in the deep UV region. The substitution of S with Se leads to band broadening, accompanied by red shifts in the absorption maxima of 20 nm for compound **2** and 15 nm for compound **4** (see Fig. 2 and Table 2).

Quantum chemical calculations of accurate energies of electronically excited states of complex organic molecules are still challenging [141]. It is known that Generalized Gradient Approximation (GGA) type functionals are more suitable for describing the UV–Vis absorption of simple aromatic molecules than Global Hybrid (GH) ones [142]. Indeed, TD-DFT calculations reveal that the absorption spectra of **1** and **2** are significantly better reproduced using GGA functional BLYP; whereas those of **3** and **4**, by GH functional B3LYP. The calculations suggest that the $S_0 \rightarrow S_1$ vertical transition in **1**–**4** corresponds to the HOMO → LUMO transition and thereby a $1\pi\pi^*$ character of the S_1 state (Table 2; ESI).

The emission of fused 1,2,5-chalcogenadiazoles is molecular-structure- and aggregation-state-dependent (and in solution, solvent-dependent); thereby, it is tunable [16,43,73–75,77,129,138–140]. For some derivatives of **5**, room-temperature red PH is reported [85,140,143–145]. Compounds **1**–**4** emit in the blue spectral region, with maximum emission wavelengths λ_{max} ranging in solution from 400 to 450 nm; the emission spectra exhibit Stokes shifts of about 4200 cm^{-1} for **1**, 3800 cm^{-1} for **2**, 800 cm^{-1} for **3**, and 2700 cm^{-1} for **4**; these shifts are smaller those for **5** and **6** (Fig. 3, Table 2). The substitution of S with Se induces a red shift in the emission maximum by 18 nm for **2** and by 45 nm for **4**. The emission spectra of **3** show a multiband shape caused by vibronic structure in the excited state. The excited-state lifetimes were determined from photoluminescence decays recorded upon pulsed laser excitation at 376 nm for **2** and 405 nm for **3** and **4**. The obtained kinetic traces were well-fitted by either bi- or mono- (**4**) exponential models (ESI) yielding the short lifetime τ_1 ~1 ns (ns) for **3** and **4**, and ~2 ns for **2**; while long-time component τ_2 is ~9 ns for **2** and ~7 ns for **3** (Table 2). Generally, small organic dyes have lifetimes in the range of ~0.1–20 ns. Overall, the findings suggest that the emission of **2**–**4** have a

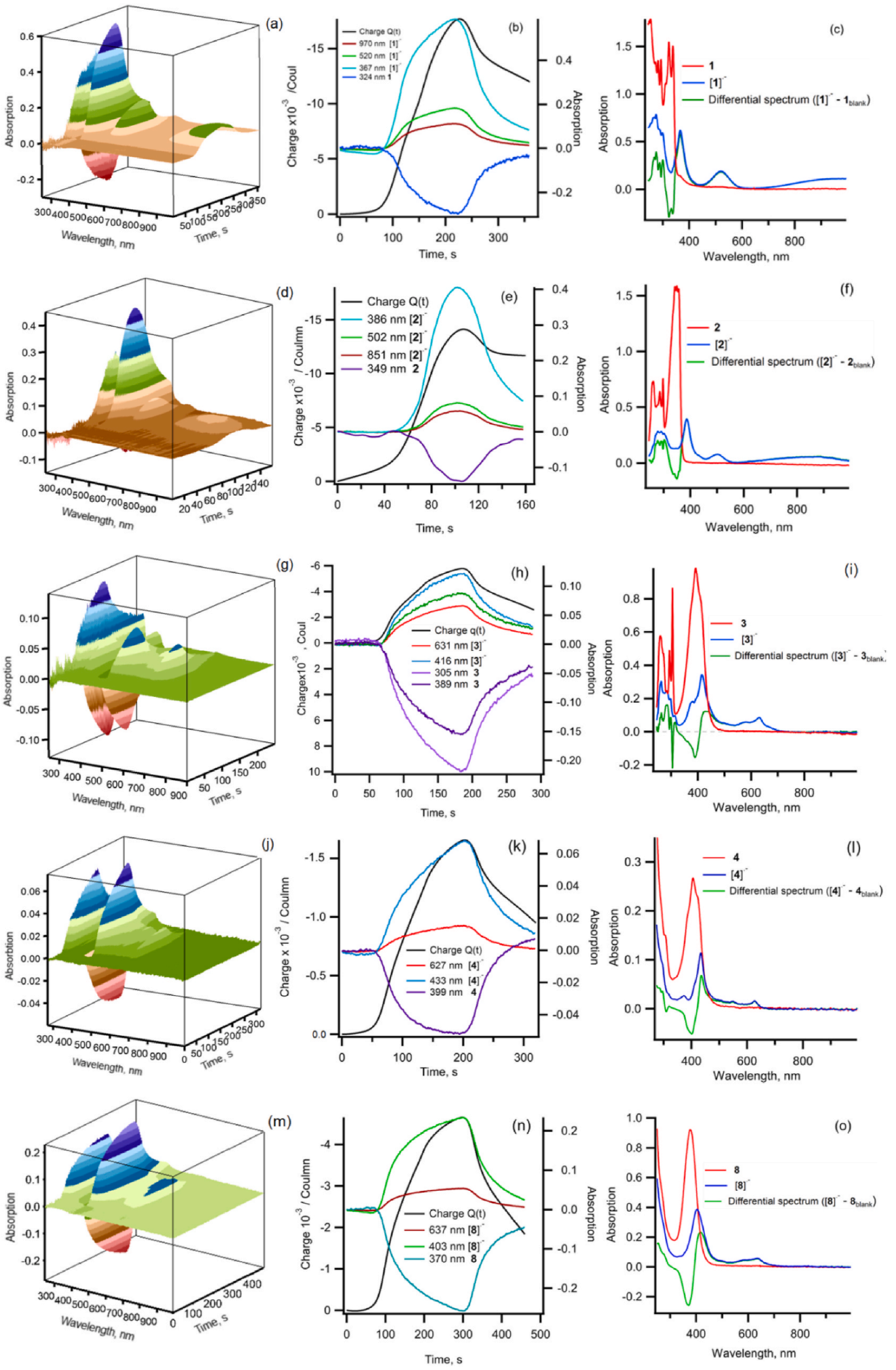

Fig. 6. (*a, d, j, g, m*) 3D UV–Vis–NIR differential reduction SEC surfaces of **M** in MeCN; (*b, e, h, k, n*) time dependence of the charge passed during electrolysis (left axes), together with the corresponding kinetics of the selected optical absorption bands (right axes); (*c, f, i, e, o*) colour-indicated electronic absorption spectrum of **M**, optical absorption spectra measured at the maxima of the charge time traces, and UV–Vis–NIR spectra of $[\mathbf{M}]^{\cdot-}$ calculated using equations (1)–(3); (**M** = **1**–**4**, **8**). (For interpretation of the references to colour in this figure legend, the reader is referred to the Web version of this article.)

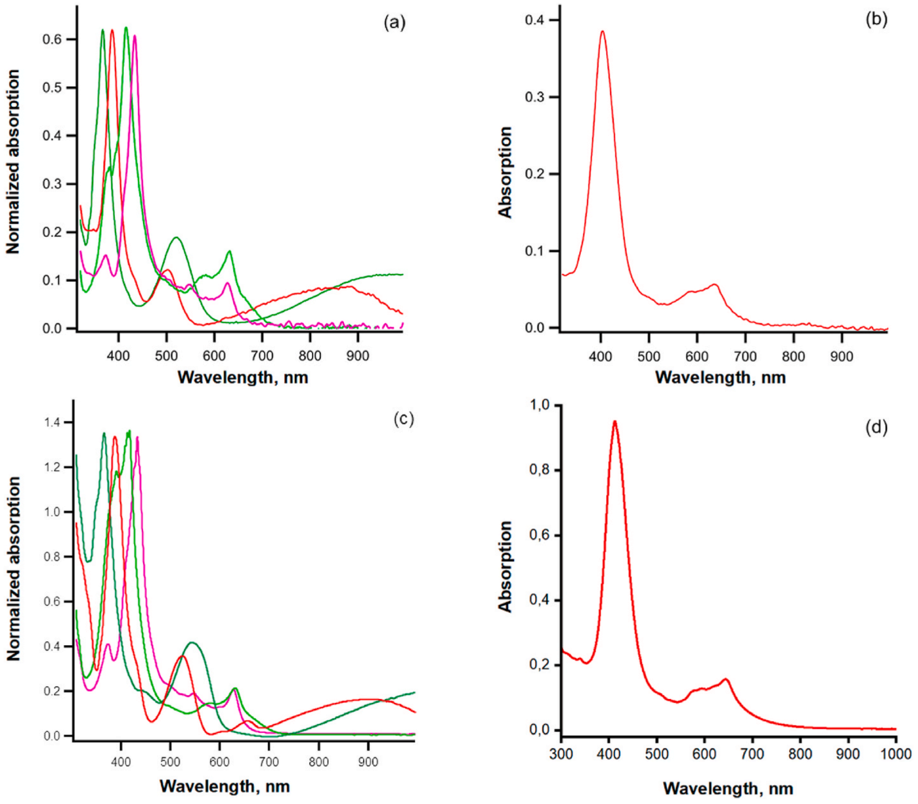

Fig. 7. Normalized Vis-NIR spectra of $[\mathbf{M}]^{\cdot-}$ from SEC (*a*, *b*) and chemical reduction (*c*, *d*): $\mathbf{M} = \mathbf{1}$–$\mathbf{4}$ (*a*, *c*), **8** (*b*, *d*); for neutral **M**, see Fig. 2, Table 2. Color code for (*a*, *c*): $[\mathbf{1}]^{\cdot-}$ green, $[\mathbf{2}]^{\cdot-}$ red, $[\mathbf{3}]^{\cdot-}$ light green, and $[\mathbf{4}]^{\cdot-}$ magenta. (For interpretation of the references to colour in this figure legend, the reader is referred to the Web version of this article.)

Table 5
Wavelengths λ_{max}/extinction coefficients log ε at the maxima of UV–Vis–NIR spectra of $[\mathrm{M}]^{\cdot-}$ in MeCN from SEC (M = 1–4, 8) and chemical reduction in MeCN (M = 3, 4) and thf (M = 1, 2, 8).

$[\mathrm{M}]^{\cdot-}$	λ_{max}, nm/log ε	
	SEC	chemical reduction [a]
$[\mathbf{1}]^{\cdot-}$	367/4.055, 520/3.539, 900–1000 (shoulder)/3.312	372, 552, 900–1000 (shoulder)
$[\mathbf{2}]^{\cdot-}$	386/4.340, 502/3.635, 851 (shoulder)/3.500	395, 439, 535, 665, 900 (shoulder)
$[\mathbf{3}]^{\cdot-}$	380/3.761, 416/3.037, 581/3.266, 631/3.343	397/4.161, 421/4.222, 587/3.261, 640/3.413
$[\mathbf{4}]^{\cdot-}$	372/3.727, 433/4.356, 549/3.479, 627/3.499	379/3.801, 440/3.452, 555/3.474, 636/3.496
$[\mathbf{8}]^{\cdot-}$	403/4.406, 586/3.490, 637/3.571 (3.574)[b]	412/4.402, 590/3.489, 642/3.582

[a] In the form of $[\mathrm{K(18\text{-}crown\text{-}6)}]^{+}[\mathbf{M}]^{\cdot-}$ salts. Reducing agents: elemental K in thf (M = **1**, **2**), PhOK in MeCN (**M** = **3**, **4**), KC_8 in thf (**M** = **8**). Extinction coefficients of $[\mathbf{1}]^{\cdot-}$ and $[\mathbf{2}]^{\cdot-}$ were not determined due to their poor stability under chemical reduction in thf.

[b] Obtained by OTE method (ESI).

fluorescence nature [146,147].

Redox properties of **1** were reported previously only for reduction [12,148]; however, EPR spectrum of $[\mathbf{1}]^{\cdot-}$ was not presented. In this work, CV/EPR and SEC studies were performed for **1**–**4** and **8**. Electrochemical oxidation of **M** in MeCN showed irreversible multi-electron oxidation peaks in (**M** = **2**–**4**) indicating the instability of their oxidized products; whereas in CH_2Cl_2 no oxidative activity was observed (**M** = **3** and **4**) in the electrochemical window of this solvent (ESI). These findings raise doubts about the possibility of obtaining long-lived $[\mathrm{M}]^{\cdot+}$ (**M** = **2**–**4**).

With electrochemical reduction, in the potential range $0 > E > -2.1$ V **1** and **2** showed a single one-electron reversible CV wave (peaks 1C-1A) associated with the formation of long-lived $[\mathbf{M}]^{\cdot-}$ (**M** = **1**, **2**) indicating an E-process of the electrochemical reduction (ECR, Fig. 3; ESI). The extension of the π-electron system in **3** and **4** leaded to EEC mechanism of the ECR associated with the formation of the long-lived $[\mathbf{M}]^{\cdot-}$ and less-stable $[\mathbf{M}]^{2-}$ (M = **3**, **4**). The $[\mathbf{3}]^{2-}$ is lesser stable than $[\mathbf{4}]^{2-}$ because the second stage of the ECR of **3** becomes reversible at the potential sweep rate $\nu > 0.3$ V s^{-1}, whereas the second CV wave of **4** is reversible over the whole range of ν studied (Fig. 4). The CV of **8** showed a reversible one-electron CV wave in the potential range $E < -1.2$ V, and an EEC process in the expanded potential range $E > -1.2$ V; the second ECR stage is essentially irreversible, indicating the instability of $[\mathbf{8}]^{2-}$ (Fig. 4). The peak and $E_{1/2}$ potentials of **3** and **4** are significantly less negative than those of **1** and **2** (Table 3). In accordance with the general trend [61], the potentials in pairs **1** and **2**, and **3** and **4**, exhibit less negative values for Se derivatives as compared with S ones. The $E_{1/2}$ potentials perfectly correlate with the DFT-calculated $a\mathrm{EA}_1$ (Tables 1 and 3; ESI). The identity of $[\mathbf{M}]^{\cdot-}$ was confirmed by EPR (Fig. 5; ESI) under conditions of potentiostatic electrolysis of **M** (**M** = **1**–**2**, **8**) in MeCN, CH_2Cl_2, or $Me_2S{=}O$, together with DFT calculations (Table 4); CH_2Cl_2 and $Me_2S{=}O$ were used due to the low solubility of the corresponding precursors **M** in MeCN. According to EPR, $[\mathbf{M}]^{\cdot-}$ (M = **1**–**4**) possess a planar rigid structure, *i.e.*, they are π-radicals. For $[\mathbf{M}]^{\cdot-}$, some hyperfine coupling (hfc) constants a^{1}H are smaller than the EPR experimental linewidths; those were estimated by simulation (Table 4). The a^{14}N indicate C_{2V} symmetry of $[\mathbf{M}]^{\cdot-}$ (M = **1**–**4**) and C_s symmetry of $[\mathbf{8}]^{\cdot-}$. According to DFT, the charge and spin densities of $[\mathbf{M}]^{\cdot-}$ (**M** = **1**–**4**) are concentrated at their heterocyclic moieties (ESI).

For the first reversible reduction CV waves (Fig. 4), the SEC surfaces representing the time-dependent superposition of UV–Vis–NIR spectra of **M** and $[\mathbf{M}]^{\cdot-}$ (M = **1**–**4**, **8**) were obtained (Fig. 6; ESI). For all **M** in

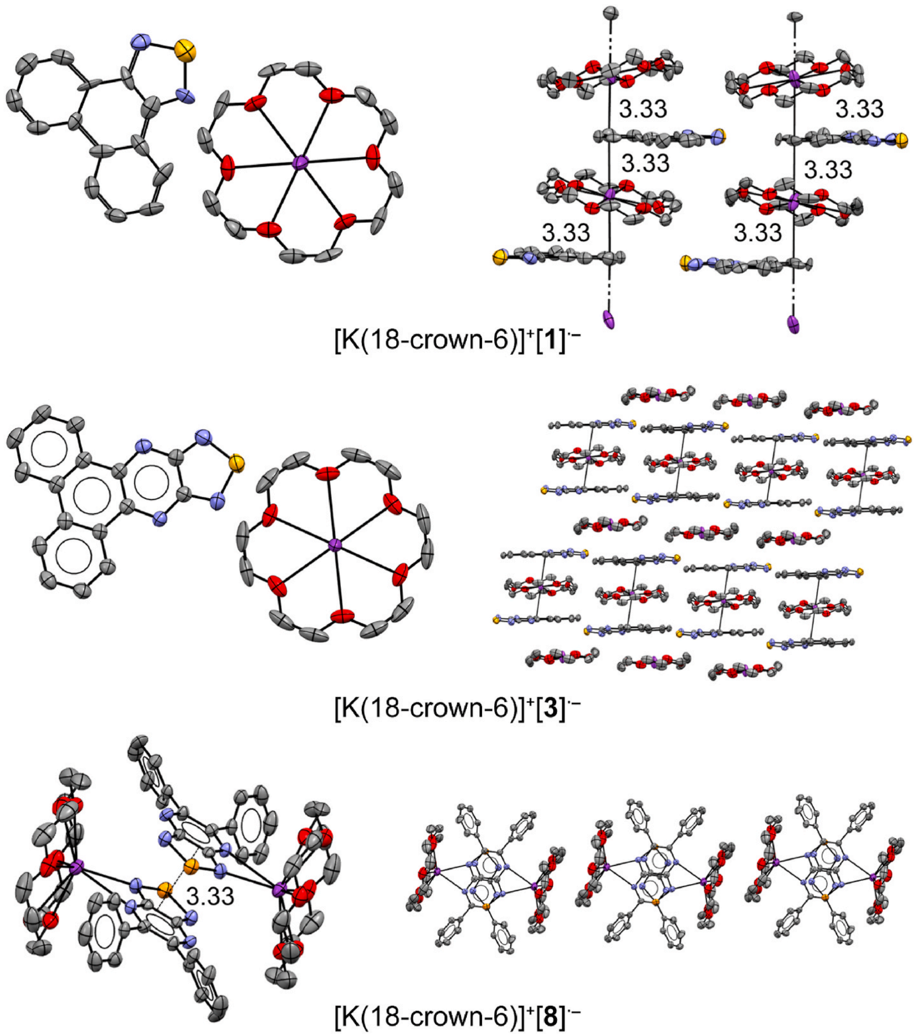

Fig. 8. XRD molecular structures and fragments of crystal structures of $[\mathrm{K(18\text{-}crown\text{-}6)}]^{+}[\mathbf{M}]^{\cdot-}$ ($\mathbf{M} = \mathbf{1}$, CCDC 2338056; **3**, CCDC 2338057; **8**, CCDC 2338058). Shortened intermolecular contacts in the crystal structures (Å): $\mathbf{M} = \mathbf{1}$, K···π 3.33; **3**, K···π 3.36–3.63; **8**, K···N 2.82–2.94, π···π 3.33. Color code (H atoms omitted): C grey, K purple, N blue, O red, S yellow. (For interpretation of the references to colour in this figure legend, the reader is referred to the Web version of this article.)

MeCN, the $\mathbf{M} \rightarrow [\mathbf{M}]^{\cdot-}$ transformation under cyclic electrolysis in the given potential sweep range at $\nu = 5$ mV s^{-1} was incomplete. Taking into account the fully reversible processes observed at the first ECR stages for all **M** (Fig. 4), the amount of $[\mathbf{M}]^{\cdot-}$ formed during the cyclic electrolysis at time t (C_t^{RA}) was estimated as follows [149]:

$$C_t^{RA} = \frac{-Q_{t0}^{t}}{(n \times F \times V)} \tag{1}$$

$$Q_{t0}^{t} = \int_{t0}^{t} I(t)dt \tag{2}$$

where Q_{t0}^{t} is the charge transferred through the SEC cell during the time from the beginning of $[\mathbf{M}]^{\cdot-}$ formation to the maximum on the charge time trace $Q(t)$ (Fig. 6); $n = 1$ is the number of electrons transferred; F is the Faraday constant, V is the effective volume of the cathode part of the SEC cell, in which the forming $[\mathbf{M}]^{\cdot-}$ is assumed to be uniformly distributed during electrolysis due to the low potential sweep rate [149]; and $I(t)$ is the SEC macroelectrolysis curve (ESI).

For the reversible process, the spectral profile of the SEC differential surface at time t is $D_t^{diff}(\lambda) = D_t^{RA}(\lambda) - D_t^{Neu}(\lambda)$, where $D_{t=0}^{Neu}(\lambda) = \varepsilon^{Neu}(\lambda) C_0^{Neu} \cdot l$ is the blank in the differential mode of the SEC experiment ($l = 0.2$ cm is the optical path). Taking into account the equal amounts of the formed $[\mathbf{M}]^{\cdot-}$ and the loss of the initial **M**, *i.e.*, $C_t^{RA} = C_t^{Neu}$, and formulae (1) and (2), the electronic absorption spectrum (EAS) of $[\mathbf{M}]^{\cdot-}$ is calculated as follows:

$$D_t^{RA}(\lambda) = D_t^{diff}(\lambda) + \frac{-Q_{t0}^{t}}{FVC_0^{Neu}} D_{t=0}^{Neu}(\lambda) \tag{3}$$

where $D_{t=0}^{Neu}(\lambda)$ is the optical spectrum of the starting compound obtained in normal mode (Fig. 6). The extinction coefficients of RA at the absorption band maxima, $\varepsilon^{RA}(\lambda_i)$, were calculated as follows:

$$\varepsilon^{RA}(\lambda_i) = \frac{FV}{-Q_{t0}^{t} \cdot l} D_t^{RA}(\lambda_i) \tag{4}$$

where $D_t^{RA}(\lambda_i)$ is the optical absorption at the maximum of the absorption band. For calculations, the maximum value of $|Q(t)|$ in the corresponding dependences was taken (Fig. 6).

The $[\mathbf{M}]^{\cdot-}$ ($\mathbf{M} = \mathbf{1}$, **3**, **8**) observed by EPR after electrochemical generation (for $[\mathbf{8}]^{\cdot-}$, see also [38]) and UV–Vis–NIR, were prepared by chemical reduction of **M** with elemental K, KC_8, or KSPh in the presence of cyclic polyether 18-crown-6 (cf. [54,55,150,151]). The authenticity of $[\mathbf{M}]^{\cdot-}$ was confirmed by EPR, and they were isolated in the form of thermally-stable $[\mathrm{K(18\text{-}crown\text{-}6)}]^{+}[\mathbf{M}]^{\cdot-}$ salts and characterized by XRD (below). Comparison of UV–Vis–NIR spectra of the salts with those from SEC confirms assignment of the latter to $[\mathbf{M}]^{\cdot-}$ (Fig. 7, Table 5). In the $300 < \lambda < 1000$ nm spectral area, absorption bands of $[\mathbf{M}]^{\cdot-}$ ($\mathbf{M} = \mathbf{1}$–**4**, **8**) are Δλ bathochromically shifted with respect to those of **M** (Fig. 3, Table 2). The Δλ and *a*EA_1 values correlate: for example, the intense absorption band in the range 367 < 433 nm shifts bathochromically on passing from S containing $[\mathbf{1}]^{\cdot-}$ to Se containing $[\mathbf{2}]^{\cdot-}$, and on passing from $[\mathbf{1}]^{\cdot-}$ and $[\mathbf{2}]^{\cdot-}$ to π-extended $[\mathbf{3}]^{\cdot-}$ and $[\mathbf{4}]^{\cdot-}$ (Fig. 7). This trend resembles that which was observed for 2,1,3-benzochalcogenadiazoles (chalcogen = S, Se, Te) [61]. The spectra of $[\mathbf{1}]^{\cdot-}$ and $[\mathbf{2}]^{\cdot-}$ exhibit a noticeable absorption in Vis-NIR area, whereas those of $[\mathbf{3}]^{\cdot-}$ and $[\mathbf{4}]^{\cdot-}$ do not. The $[\mathbf{8}]^{\cdot-}$ also did not reveal a noticeable NIR absorption (Fig. 7).

XRD structures of $[\mathrm{K(18\text{-}crown\text{-}6)}]^{+}[\mathbf{M}]^{\cdot-}$ exhibit stacks (**M** = **1**) or layers (**M** = **3**) with coplanar orientation of $[\mathrm{K(18\text{-}crown\text{-}6)}]^{+}$ and $[\mathbf{M}]^{\cdot-}$ (Fig. 8). This orientation is markedly different from the packing modes of previously studied RA salts with $[\mathrm{K(18\text{-}crown\text{-}6)}]^{+}$, where RAs are typically involved in shortened K···N electrostatic contacts [6]. In contrast, the structure of $[\mathrm{K(18\text{-}crown\text{-}6)}]^{+}[\mathbf{8}]^{\cdot-}$ contains π-dimers of $[\mathbf{8}]^{\cdot-}$ (π···π contact, 3.33 Å) similar to those of two other 1,2,5-chalcogenadiazolidyl RAs (3.18 Å, chalcogen = Se [151]; 3.25 Å, chalcogen = S [152]; the sum of VdW radii of two E atoms is 3.54, 3.64, 3.78 Å for E = C, S, Se, respectively [131].

In contrast to previously studied 1,2,5-chalcogenadiazoles [6,100, 153–155], **1**–**4** do not form CT complexes with tetrathiafulvalene under conditions of cocrystallization from organic solvents.

4. Conclusions

This study, based on TG-DSC, XRD, UV–Vis–NIR/FL, CV, EPR, and SEC measurements, together with DFT and TD-DFT calculations, and performed on neutral **M** and reduced $[\mathbf{M}]^{\cdot-}$ states of 1,2,5-thia/selenadiazoles **1**–**4** suggests that according to the thermal, structural, optical, and redox properties **1**–**4** are promising small-molecule organic dyes/non-fullerene electron acceptors for optoelectronics. Their advantages embrace synthetic availability, planar π-extended molecular structures, absorption and emission of visible light, low reduction potentials, and reversible RA states, whose UV–Vis–NIR spectra are different from those of the neutral precursors. DFT-calculated *a*IE_1 of **1**–**4** is practically constant as 7.9 ± 0.1 eV, whereas *a*EA_1 varies on a broad scale from 0.82 to 2.13 eV. The experimentally estimated energy gap ΔE between the highest occupied and the lowest unoccupied electronic levels is narrower for **3** and **4** (~2.7–2.8 eV) than for **1** and **2** (~3.3–3.4 eV). It is found that π-extension, provoking red shifts in UV–Vis and FL spectra of polycyclic **1**–**4** and decrease of ECR potentials as compared with their bicyclic archetypes **5** and **6**, has its limitation as a tool for the tuning of *a*EA_1 values. The redox and optical properties of **1**–**4** also depend on the nature of chalcogen atoms, and replacement of S by Se also works for red shift of UV–Vis and FL bands and decrease of ECR potentials; with Se derivatives, SOC can potentially be involved in optoelectronic properties. These findings can be used in molecular design of new small-molecule dyes, as well as pendant electron-acceptor groups of electroactive polymers [156–158], for organic optoelectronics. Overall, compounds **1**–**4** exhibit more favorable combination of functional properties, especially redox and photophysical ones, as compared with reference compounds **5**–**9**.

In the context of further molecular design, it should be noted that the frontier MOs of **1**–**4** are energetically and spatially closed (ESI); the latter in the sense that they are localized in the same spatial area inside the molecular VdW surface. With carbocyclic substitution, it looks possible to achieve spatial separation of the frontier MOs conserving their energetic proximity, *i.e.*, transform **1**–**4** into highly promising multiresonant fluorophores [159,160]. This can be one of directions of further design and synthesis.

In the chalcogen context, Te analogs, which are generally promising [35,61], in the case of 1,2,5-telluradiazoles exhibit disadvantages associated with low solubility and volatility caused by strong Te···N *ChB* [47,49–51,57,116], as well as instability towards atmospheric moisture [5]. In further work, other than the aforementioned functionalized derivatives of **1**–**4**, *e. g.* partially or fully halogenated (halogen = F, Cl), also worth special attention. Specifically, solid halogenated aromatics frequently exhibit well-ordered structures controlled by polyhaloarene-polyhaloarene (halogen = F, Cl) π-stacking [161–164] similar to better studied arene-polyfluoroarene [165] (or, broader, arene-polyhaloarene [166]) π-staking, which in the case of 1,2,5-chalcogenadiazoles might be in cooperativity with lateral *ChB*. Also halogenation frequently improves functional properties [167–173]; particularly, Stocks shifts for tetrafluorinated derivatives of **5** and **6** are larger than for the parent compounds [174]. And fluorinated polycyclic chalcogen-nitrogen heteroaromatics possess stable RA states [65,175].

CRediT authorship contribution statement

Ekaterina A. Radiush: Visualization, Investigation, Funding acquisition, Formal analysis, Data curation. **Vladislav M. Korshunov:** Writing – original draft, Investigation, Formal analysis, Data curation. **Elena A. Chulanova:** Investigation, Formal analysis, Data curation. **Lidia S. Konstantinova:** Investigation, Formal analysis, Data curation. **Alexey I. Ferulev:** Investigation, Formal analysis, Data curation. **Irina G. Irtegova:** Visualization, Investigation, Formal analysis, Data curation. **Inna K. Shundrina:** Investigation, Formal analysis, Data curation. **Ekaterina A. Frank:** Investigation, Data curation. **Nikolay A. Semenov:** Investigation, Formal analysis, Data curation. **Ilya V. Taidakov:** Investigation, Data curation. **Oleg A. Rakitin:** Investigation, Formal analysis, Data curation. **Leonid A. Shundrin:** Writing – original draft, Visualization, Supervision, Methodology, Investigation, Formal analysis, Data curation, Conceptualization. **Andrey V. Zibarev:** Writing – original draft, Supervision, Project administration, Formal analysis, Data curation, Conceptualization.

Declaration of competing interest

The authors declare that they have no known competing financial interests or personal relationships that could have appeared to influence the work reported in this paper.

Acknowledgements

The authors are grateful to Prof. Irina Yu. Bagryanskaya for preliminary XRD measurements on $[\mathrm{K(18\text{-}crown\text{-}6)}]^{+}[\mathbf{8}]^{\cdot-}$, and to the Russian Science Foundation (project no. 24-73-00367; synthesis, XRD, and UV–Vis) and the Ministry of Higher Education and Science of the Russian Federation (research program FWUE-2025-0007; CV, EPR, and spectroelectrochemistry) for financial support. The Multi-Access Chemical Research Centre, Siberian Branch of the Russian Academy of Sciences, is gratefully acknowledged for instrumental facilities.

Appendix A. Supplementary data

Supplementary data to this article can be found online at https://doi.org/10.1016/j.dyepig.2025.112922.

Data availability

No data was used for the research described in the article.

References

[1] Varghese MA, Anjali A, Harshini D, Nagarajan S. Organic light-emitting transistors: from understanding to molecular design and architecture. ACS Appl Electron Mater 2021;3:550–73. https://doi.org/10.1021/acsaelm.0c00931.

[2] Gierschner J, Shi J, Roca-Sanjuán D, Milián-Medina B, Varghese S, Park SY. Luminescence in crystalline organic materials: from molecules to molecular solids. Adv Opt Mater 2021;9:2002251. https://doi.org/10.1002/adom.202002251.

[3] Jiang Y, Liu YY, Liu X, Lin H, Gao K, Lai WY, Huang W. Organic solid-state lasers: a materials view and future development. Chem Soc Rev 2020;49:5885–944. d0cs00037j.

[4] Chivers T, Laitinen RS. Chalcogen-nitrogen chemistry: from fundamentals to applications in biological, physical, and materials sciences. World Scientific 2021. https://doi.org/10.1142/12397.

[5] Rakitin OA, Zibarev AV. Synthesis and applications of 5-membered chalcogen-nitrogen π-heterocycles with three heteroatoms. Asian J Org Chem 2018;7: 2397–416. https://doi.org/10.1002/ajoc.201800536.

[6] Chulanova EA, Semenov NA, Pushkarevsky NA, Gritsan NP, Zibarev AV. Charge-transfer chemistry of chalcogen-nitrogen π-heterocycles. Mendeleev Commun 2018;28:453–60. https://doi.org/10.1016/j.mencom.2018.09.001.

[7] Rakitin OA. Fused 1,2,5-thia- and 1,2,5-selenadiazoles: synthesis and applications in materials chemistry. Tetrahedron Lett 2020;61:152230. https://doi.org/10.1016/j.tetlet.2020.152230.

[8] Rakitin OA. 1,2,5-Thiadiazoles. In: Koutentis PA, editor. Comprehensive heterocyclic chemistry IV, vol. 5. Elsevier; 2022. p. 371–406. https://doi.org/10.1016/b978-0-12-409547-2.14813-9.

[9] Yamazaki S. Three or four heteroatoms including at least one selenium or tellurium. In: Smith JA, editor. Comprehensive heterocyclic chemistry IV, vol. 6. Elsevier; 2022. p. 303–409. https://doi.org/10.1016/b978-0-12-818655-8.00053-6.

[10] Rakitin OA. Recent developments in the synthesis of 1,2,5-thiadiazoles and 2,1,3-benzothiadiazoles. Synthesis 2019;51:4338–47. https://doi.org/10.1055/s-0039-1690679.

[11] Cillo CM, Lash TD. Benzo[1,2-*c*:3,4-*c*']bis[1,2,5]selenadiazole, [1,2,5]selenadiazolo[3,4-*e*]-2,1,3-benzothiadiazole, furazanobenzo-2,1,3-thiadiazole, furazanobenzo-2,1,3-selenadiazole and related heterocyclic systems. J Heterocycl Chem 2004;41:955–62. https://doi.org/10.1002/jhet.5570410616.

[12] Linder T, Badiola E, Baumgartner T, Sutherland TC. Synthesis of π-extended thiadiazole (oxides) and their electronic properties. Org Lett 2010;12:4520–3. https://doi.org/10.1021/ol1018213.

[13] Gang W, Zhao D, Chen F, Zhao J, Bu J, Zhou Z, Gou S, Xu G. Near infrared-triggered dibenzo[*a*,*c*][1,2,5]thiadiazolo[3,4-*i*]phenazine heterocyclic derivatives for type-I photodynamic and photothermal therapy against human nasopharyngeal carcinoma. Dyes Pigments 2024;226:112133. https://doi.org/10.1016/j.dyepig.2024.112133.

[14] Dias GG, Soto FT, Machado VG. 2,1,3-Benzothiadiazoles are versative fluorophore building blocks for the design of analyte-sensing optical devices. Chemosensors 2024;12:156. https://doi.org/10.3390/chemosensors12080156.

[15] Liu R, Zhou C, Ding Q, Qu L, Wang K, Tang H, Li Y, Yang C. Dual-state emission of D–A–D type benzothiadiazole derivatives for the sensitive detection of amine compounds. Dyes Pigments 2023;219:111588. https://doi.org/10.1016/j.dyepig.2023.111588.

[16] Posada Urritia M, Dyrager C. Tuning emission properties of 2,1,3-benzothiadiazoles via regioselecttive substitution. Chem Eur J 2024;30:e20240644. https://doi.org/10.1002/chem.202400644.

[17] Elnagdy HMF. 4,7-Di(2-thienyl)-2,1,3-benzothiadiazole DTBT as active core for synthesizing small molecules to optoelectronic applications: a review. Dyes Pigments 2024;229:112251. https://doi.org/10.1016/j.dyepig.2024.112251.

[18] Warner CC, Thooft AM, Norris SR, Lampkin BJ, Demirci SK, VanVellet B. The malleable excited states of benzothiadiazole dyes and investigation of their potential for photochemical control. ChemistrySelect 2020;5:7016–20. https://doi.org/10.1002/slct.202001980.

[19] Martin K, Aharon T, Mastropasqua Talamo M, Hauser A, Bürgi T, Vanthuyne N, Caricato M, Avarvari N. Helicene appended benzothiadiazoles as chiral emitters. Chem Eur J 2024;30:e202401413. https://doi.org/10.1002/chem.202401413.

[20] Biet T, Martin K, Kankache J, Hellou N, Hauser A, Bürgi T, Vanthuyne N, Aharon T, Caricato M, Crassous J, Avarvari N. Triggering emission with the helical turn in thiazole-helicenes. Chem Eur J 2017;23:437–46. https://doi.org/10.1002/chem.201604471.

[21] Yu Z, Shi G, Wang KP, Xu LZ, Chen S. Benzothiadiazole-derived double aza[5]helicenes: synthesis, crystal structures, and optical properties. Tetrahedron 2023;130:133178. https://doi.org/10.1016/j.tet.2022.133178.

[22] Zhang Z, Murata Y, Hirose T. Circularly polarized luminescence of hetero[n]helicenes with 2,1,3-benzothiadiazole rings at both ends: design of magnetically-allowed electronic transitions via heteroatom embedding. Tetrahedron 2023;142:133514. https://doi.org/10.1016/j.tet.2023.133514.

[23] Duan T, Feng W, Li Y, Li Z, Zhang Z, Liang H, Chen H, Zhong C, Jeong J, Yang C, Chen S, Lu S, Rakitin OA, Li C, Ban X, Kan B, Chen Y. Electronic configuration tuning of centrally extended non-fullerene acceptors enabling organic solar cells with efficiency approaching 19%. Angew Chem Int Ed 2023;62:e202308832. https://doi.org/10.1002/anie.202308832.

[24] Zhu JJ, Liu G, Pang JH, Li MD, Wang Y, Tang QX. Benzothiadiazole hot exiton materials for red electroluminescence with the maximum external quantum efficiency approaching 10%. J Mater Chem C 2022;10:8684–93. https://doi.org/10.1039/d2tc01233b.

[25] Tam TLD, Wu J. Benzo[1,2-*c*;4,5-*c*']bis[1,2,5]thiadiazole in organic optoelectronics: a mini-review. J Mol Eng Mater 2015;3:1540003. https://doi.org/10.1142/S2251237315400031.

[26] Korshunov VM, Chmovzh TN, Knyazeva EA, Taydakov IV, Mikhalchenko LV, Varaksina EA, Saifuyarov RS, Avetissov IG, Rakitin OA. A novel candle light-style OLED with a record low colour temperature. Chem Commun 2019;55:13354–7. https://doi.org/10.1039/c9cc04973h.

[27] Liu Z, Jiang C, Chen X, Song G, Wan X, Kan B, Duan T, Knyazeva EA, Rakitin OA, Chen Y. Side-chain modifications of non-fullerene acceptors for organic solar cells with efficiency over 18%. J Mater Chem C 2023;11:6920–7. https://doi.org/10.1039/d3tc00820g.

[28] Misra R, Gautam P. Tuning of the HOMO-LUMO gap of donor-substituted symmetrical and unsymmetrical benzothiadiazoles. Org Biomol Chem 2014;12: 5448–57. https://doi.org/10.1039/c4ob00629a.

[29] Gautam P, Maragani R, Misra R. Aryl-substituted symmetrical and unsymmetrical benzothiadiazoles. RSC Adv 2015;5:18288–94. https://doi.org/10.1039/c4ra15424j.

[30] Mota AAR, Carvalho PHPR, Guido BC, de Oliveira HCB, Soares TA, Corrêa JR, Neto BAD. Bioimaging, cellular uptake and dynamics in living cells of lipophilic fluorescent benzothiadiazole at low temperature (4^{o}C). Chem Sci 2014;5: 3995–4003. https://doi.org/10.1039/c4sc01785d.

[31] Carvalho PHPR, Corrêa JR, Guido BC, Gatto C, de Oliveira HCB, Soares TA, Corrêa JR, Neto BAD. Designed benzothiadiazole fluorophores for selective mitochondrial imaging and dynamics. Chem Eur J 2014;20:15360–73. https://doi.org/10.1002/chem.201404039.

[32] Paramasivam M, Gupta A, Raynor AM, Bhosale SV, Bhanuprakash K, Rao J. Small band gap D–π–A–π–D benzothiadiazole derivatives with low-lying HOMO levels as potential donors for applications in organic photovoltaics: a combined experimental and theoretical investigation. RSC Adv 2014;4:35318–31. https://doi.org/10.1039/c4ra02700k.

[33] Jiang D, Chen S, Xue Z, Li Y, Liu H, Yang W, Li Y. Donor-acceptor molecules based on benzothiadiazole: synthesis, X-ray crystal structures, linear and third-order nonlinear optical properties. Dyes Pigments 2016;125:100–5. https://doi.org/10.1016/j.dyepig.2015.10.014.

[34] Miranda MS, Matos MAR, Morais VMF, Liebman JF. 2,1,3-Benzothiadiazole: study of its structure, energetics and aromaticity. J Chem Thermodyn 2012;50: 30–6. https://doi.org/10.1016/j.ict.2012.02.005.

[35] Pritchina EA, Gritsan NP, Rakitin OA, Zibarev A. V. 2,1,3-Benzochalcogenadiazoles: regularities and peculiarities over a whole chalcogen pentad O, S, Se, Te and Po. Targets Heterocycl. Off Syst 2019;23:143–54. https://doi.org/10.17374/targets.2020.23.143.

[36] An C, Zhou S, Baumgarten M. Condensed derivatives of thiadiazoloquinoxaline as strong acceptors. Cryst Growth Des 2015;15:1934–8. https://doi.org/10.1021/acs.cgd.5b00105.

[37] Mori H, Nishinaga S, Takahashi R, Nishihara Y. Alkoxy-substituted anthra[1,2-c:5,6-*c*']bis([1,2,5]thiadiazole) (ATz): a new electron-acceptor unit in the semiconducting polymers for organic electronics. Macromolecules 2018;51: 5473–84. https://doi.org/10.1021/acs.macromol.8b01230.

[38] Konstantinova LS, Bobkova IE, Nelyubina YV, Chulanova EA, Irtegova IG, Vasilieva NV, Camacho PS, Ashbrook SE, Hua G, Slawin AMZ, Woollins JD, Zibarev AV, Rakitin OA. [1,2,5]Selenadiazolo[3,4-*b*]pyrazines: synthesis from 3,4-diamino-1,2,5-selenadiazole and generation of persistent radical anions. Eur J Org Chem 2015;2015:5585–93. https://doi.org/10.1002/ejoc.201500742.

[39] Alfuth J, Zadykowicz B, Sikorski A, Połoński T, Eichstaedt K, Olszewska T. Effect of aromatic system expansion on crystal structures of 1,2,5-thia- and 1,2,5-selenadiazoles, and their quaternary salts: synthesis, structure, and spectroscopic properties. Materials (Basel) 2020;13:4908. https://doi.org/10.3390/ma13214908.

[40] Kato S, Furuya T, Nitani M, Hasebe N, Ie Y, Aso Y, Yoshihara T, Tobita S, Nakamura Y. A series of π-extended thiadiazoles fused with electron-donating heteroaromatic moieties: synthsis, properties, and polymorphic crystals. Chem Eur J 2015;21:3115–28. https://doi.org/10.1002/chem.201405478.

[41] Stuzhin PA, Mikhailov MS, Yurina ES, Bazanov MA, Koifman OI, Pakhomov GL, Travkin VV, Sinelshchikova AA. First tellurium-containing phthalocyanine analogues: strong effect of tellurium on spectral, redox, and conductivity properties of porphyrazines with annulated chalcogenadiazole ring(s). Chem Commun 2012;48:10135–7. https://doi.org/10.1039/c2cc35580a.

[42] Svec J, Zimcik P, Novakova L, Rakitin OA, Amelichev SA, Stuzhin PA, Novakova V. 1,2,5-Chalcogenadiazole-annulated tripyrazinoporphyrazines: synthesis, spectral characteristics, and influence of the heavy atom effect on their photophysical properties. Eur J Org Chem 2015;2015:596–604. https://doi.org/10.1002/ejoc.201403329.

[43] Korshunov VM, Chmovzh TN, Tsorieva AV, Gruzdev GA, Rakhimkulov DM, Taydakov IV, Rakitin OA. Towards deep NIR emissive simple D–A–D dyes: a novel acceptor block providing anti-kasha's rule emission. J Mater Chem C 2024;12: 19200–11. https://doi.org/10.1039/d4tc03132f.

[44] Chulanova EA, Radiush EA, Shundrina IK, Iyu Bagryanskaya, Semenov NA, Beckmann J, Gritsan NP, Zibarev AV. Lewis ambiphilicity of 1,2,5-chalcogenadiazoles for crystal engineering: complexes with crown ethers. Cryst Growth Des 2020;20:5868–79. https://doi.org/10.1021/acs.cgd.0c00536.

[45] Vogel L, Wonner P, Huber SM. Chalcogen bonding: an overview. Angew Chem Int Ed 2019;58:1880–91. https://doi.org/10.1002/anie.201809432.

[46] Pati PB. 2E–2N squares: chalcogen (E = S, Se, Te) bonding involving benzochalcogenadiazoles. Asian J Org Chem 2023;12:e202300056. https://doi.org/10.1002/ajoc.202300056.

[47] Radiush EA, Wang H, Chulanova EA, Prima DO, Radaeva NS, Ponomareva YA, Semenov NA, Zibarev AV. Recognition and sensing of Lewis bases by 1,2,5-chalcogenadiazoles. Mendeleev Commun 2024;34:297–306. https://doi.org/10.1016/j.mencom.2024.04.001.

[48] Semenov NA, Lonchakov AV, Gritsan NP, Zibarev AV. Donor-acceptor coordination of anions by chalcogen atoms of 1,2,5-chalcogenadiazoles. Russ Chem Bull 2015;64:499–510. https://doi.org/10.1007/s11172-015-0893-7.

[49] Ho PC, Wang JZ, Meloni F, Vargas-Baca I. Chalcogen bonding in materials chemistry. Coord Chem Rev 2020;422:213464. https://doi.org/10.1016/j.ccr.2020.213464.

[50] Tiekink ERT. Te···N secondary bonding interactions in tellurium crystals: supramolecular aggregation patterns and a comparison with lighter congeners. Coord Chem Rev 2022;457:214397. https://doi.org/10.1016/j.ccr.2021.214397.

[51] Cozzolino AF, Vargas-Baca I, Mansour S, Mahmoudkhani AH. The nature of the supramolecular association of 1,2,5-chalcogenadiazoles. J Am Chem Soc 2005; 127:3184–90. https://doi.org/10.1021/ja044005y.

[52] Pushkarevsky NA, Smolentsev AI, Wang H, Shishova VE, Chulanova EA, Wei Q, Balmohammadi Y, Radiush EA, Grabowsky S, Beckmann J, Woollins JD, Semenov NA, Zibarev AV. Coordination polymers between 3,4-dicyano-1,2,5-telluradiazole and N,N,N′,N′-tetramethylethane-1,2-diamine: the decisive role of chalcogen bonding. Cryst Growth Des 2024;24:5236–50. https://doi.org/10.1021/acs.cgd.4c00475.

[53] Radiush EA, Wang H, Chulanova EA, Ponomareva YA, Li B, Wei Q, Salnikov GE, Petrakova SY, Semenov NA, Zibarev AV. Halide complexes of 5,6-dicyano-2,1,3-benzoselenadiazole with 1:4 stoichiometry: cooperativity between chalcogen and hydrogen bonding. ChemPlusChem 2023;88:e20230053. https://doi.org/10.1002/cplu.202300523.

[54] Pushkarevsky NA, Smolentsev AI, Dmitriev AA, Vargas-Baca I, Gritsan NP, Beckmann J, Zibarev AV. Bis(2,1,3-benzotelluradiazolidyl) 2,1,3-benzotelluradiazole: a pair of radical anions coupled by Te…N chalcogen bonding. Chem Commun 2020;56:1113–6. https://doi.org/10.1039/c9cc08110k.

[55] Pushkarevsky NA, Chulanova EA, Shundrin LA, Smolentsev AI, Salnikov GE, Pritchina EA, Genaev AM, Irtegova IG, Bagryanskaya IY, Konchenko SN, Gritsan NP, Beckmann J, Zibarev AV. Radical anions, radical-anion salts and anionic complexes of 2,1,3-benzochalcogenadiazoles. Chem Eur J 2019;25: 806–16. https://doi.org/10.1002/chem.201803465.

[56] Radiush EA, Pritchina EA, Chulanova EA, Dmitriev AA, Bagryanskaya IY, Slawin AMZ, Woollins JD, Gritsan NP, Zibarev AV, Semenov NA. Chalcogen-bonded donor-acceptor complexes of 5,6-dicyano[1,2,5]selenadiazole[3,4-*b*] pyrazine with halide ions. New J Chem (1987) 2022;46:14490–501. https://doi.org/10.1039/d2nj02345h.

[57] Wei Q, Wang H, Zibarev AV. Influence of 2,1,3-pyrazinochalcogenadiazoles structure on their dimerization via chalcogen bonding (chalcogen = S, Se, Te). Comput Theor Chem 2024;1242:114984. https://doi.org/10.1016/j.comptc.2024.114984.

[58] Pushkarevsky NA, Petrov PA, Grigoriev DS, Smolentsev AI, Lee LM, Kleemiss F, Salnikov GE, Konchenko SN, Vargas-Baca I, Grabowsky S, Beckmann J, Zibarev AV. The nature of bonding in donor-acceptor interactions exemplified by complexes of N-heterocyclic carbenes with 1,2,5-telluradiazoles. Chem Eur J 2017;23:10987–91. https://doi.org/10.1002/chem.201703018.

[59] Pati PB, Zade SS. Benzoselenadiazole containing donor-acceptor-donor small molecules: nonbonding interactions, packing patterns, and optoelectronic properties. Cryst Growth Des 2014;14:1695–700. https://doi.org/10.1021/cg401830f.

[60] Miao S, Sun X, Zhang Y, Wang W. Chalcogen-bonded [Se–N]$_2$ cyclic supramolecular synthons enhanced by chalcogens bonds: studies in the gas phase and crystalline phase. Int J Mol Sci 2025;26:2324. ijms26052324.

[61] Chulanova EA, Radiush EA, Semenov NA, Hupf E, Irtegova IG, Kosenkova YS, Bagryanskaya IY, Shundrin LA, Beckmann J, Zibarev AV. Tuning molecular electron affinities against atomic electronegativities by spatial expansion of a π-system. ChemPhysChem 2023;24:e202200876. https://doi.org/10.1002/cphc.202200876.

[62] Boeré RT, Roemmele TL. Electrochemistry of redox-active group 15/16 heterocycles. Coord Chem Rev 2000;210:369–445. https://doi.org/10.1016/S0010-8545(00)00349-0.

[63] Lonchakov AV, Rakitin OA, Gritsan NP, Zibarev AV. Breathing some new life into an old topic: chalcogen-nitrogen π-heterocycles as electron acceptors. Molecules (Basel) 2013;18:9850–900. https://doi.org/10.3390/molecules18089850.

[64] Zibarev AV. Chalcogen-nitrogen heterocyclic radicals. In: Lippolis V, Santi C, Lenardão EJ, Braga AL, editors. Chalcogen chemistry: fundamentals and applications. Royal Society of Chemistry; 2023. p. 168–86. https://doi.org/10.1039/bk9781839167386-00168.

[65] Shundrin LA, Irtegova IG, Avrorov PA, Mikhailovskaya TF, Makarov AG, Makarov AY, Zibarev AV. Electrochemical reduction, radical anions, and degalogenation of fluorinated/chlorinated 2,1,3-benzothia/selenadiazoles. ARKIVOC (Gainesville, FL, U S) 2017;iii:168–80. https://doi.org/10.3998/ark.5550190.p010.

[66] Chmovzh TN, Kudryashev TA, Mikhalchenko LV, Rakitin OA. [1,2,5]Thia(selena) diazolo[3,4-*c*]pyridine-4,7-dicarbonitriles: synthesis and electrochemical reduction to radical anions. Russ Chem Bull 2024;73:1280–5. https://doi.org/10.1007/s11172-024-4244-4.

[67] Armin A, Li W, Sandberg OJ, Xiao Z, Ding L, Nelson J, Neher D, Vanderwal V, Shoaee S, Wang T, Ade H, Heumüller T, Brabec C, Meredith P. A history and perspective of non-fullerene electron acceptors for organic solar cells. Adv Energy Mater 2021;11:20003570. https://doi.org/10.1002/aenm.2020033570.

[68] Nielsen CB, Holliday S, Chen HY, Cryer SJ, McCulloch I. Non-fullerene electron acceptors for use in organic solar cells. Acc Chem Res 2015;48:2803–12. https://doi.org/10.1021/acs.accounts.5b00199.

[69] Nie Q, Tang A, Guo Q, Zhou E. Benzothiadiazole-based non-fullerene acceptors. Nano Energy 2021;87:106174. https://doi.org/10.1016/j.nanoen.2021.106174.

[70] Korshunov VM, Chmovzh TN, Freidzon AY, Minyaev ME, Barkanov AD, Golovanov IS, Mikhalchenko LV, Avetisov IG, Taydakov IV, Rakitin OA. Small D–π–A–π–D organic dyes for near-infrared emitting OLEDs with excellent external quantum efficiency. Dyes Pigments 2023;208:110860. https://doi.org/10.1016/j.dyepig.2022.110860.

[71] Rani A, Zafar F, Hussain R, Zafar W, Khanum A, Adnan M. Molecular engineering of benzothiadiazole core based non-fullerene acceptors to tune the optoelectronic properties of perovskite solar cells. Comput Theor Chem 2024;1237:114637. https://doi.org/10.1016/j.comptc.2024.114637.

[72] Sukhikh TS, Ogienko DS, Bashirov DA, Konchenko SN. Luminescent complexes of 2,1,3-benzothiadiazole derivatives. Russ Chem Bull 2019;68:651–61. https://doi.org/10.1007/s11172-019-2472-9.

[73] Neto BAD, Corrêa JR, Spencer J. Fluorescent benzothiadiazole derivatives as fluorescence imaging dyes: a decade of new generation probes. Chem Eur J 2022; 28:e202103262. https://doi.org/10.1002/chem.202103262.

[74] Neto BAD, Lapis AAM, da Silva EN, Dupont J. 2,1,3-Benzothiadiazole and derivatives: synthesis, properties, reactions, and applications in light technologies of small molecules. Eur J Org Chem 2013;2013:228–55. https://doi.org/10.1002/ejoc.201201161.

[75] Henry BR, Morrison JD. Studies of the electronic absorption and emission spectra of 2,1,3-benzothiadiazole. J Mol Spectrosc 1975;58:311–8. https://doi.org/10.1016/0022-2852(75)90271-1.

[76] Hu Z, Feng L, Yang P. 2,1,3-Benzothiadiazole derivative small molecule fluorophores for NIR-II bioimaging. Adv Funct Mater 2024;34:2310818. https://doi.org/10.1002/adfm.202310818.

[77] Medeiros GA, Corrêa JR, Barbosa ALA, Krüger R, Balagues RA, Lopes TO, de Oliveira HCB, Alves D, Neto BAD. Fluorescent benzoselenadiazoles: synthesis, characterization, and quantification of intracellular lipid droplets and multicellular model staining. J Org Chem 2020;85:10561–73. https://doi.org/10.1021/acs.joc.0c01031.

[78] Yao S, Kim B, Gomez MYC, Mv Bondar MV, Belfield KD. Synthesis of near-infrared fluorescent two-photon-absorbing fluorenyl benzothiadiazole and benzoselenadiazole derivatives. ACS Omega 2016;1:1149–56. https://doi.org/10.1021/acsomega.6b00289.

[79] Chang Q, Ding W, Chen S, Soundarajan K, Cheng X. Amphiphilic benzothiadiazole derivatives: synthesis, self-assembly and applications as light-emitting liquid crystal display and switchable anisotropic scattering device. J Mol Liq 2022;363:119832. https://doi.org/10.1016/j.molliq.2022.119832.

[80] Korshunov VM, Chmovzh TN, Golovanov IS, Knyazeva EA, Mikhalchenko LV, Saifutyarov RS, Avetisov IC, Woollins JD, Rakitin OA. Candle light-style OLEDs with benzochalcogenadiazoles cores. Dyes Pigments 2021;185:108917. https://doi.org/10.1016/j.dyepig.2020.108917.

[81] Robertson LA, Shkrob IA, Agarwal G, Zhao Y, Yu Z, Assary RS, Cheng L, Moore JS, Zhang L. Fluorescence-enabled self-reporting redox flow batteries. ACS Energy Lett 2020;5:3062–8. acsenergylett.0c01447.

[82] Ceriani C, Corsini F, Mattoli G, Mattiello S, Testa D, Po R, Batta C, Graffini G, Berita L. Sustainable by design, large Stokes shift benzothiadiazole derivatives for luminescent solar concentrators. J Mater Chem C 2021;9:14815–26. https://doi.org/10.1039/d1tc03536c.

[83] Loaeza L, Maraval V, Saquet A, Ramos-Ortiz G, Chauvin R, Farfan N. Strong absorber *vs* strong emitter in extended π-conjugated systems: a *carbo*-benzene–benzothiadiazole chromophore. New J Chem (1987) 2022;46: 6494–501. https://doi.org/10.1039/d2nj00569g.

[84] Neto JSS, Krüger R, Balaguez RA, Fronza MG, Acunha TV, Oliboni RS, Savegnago L, Iglesias BA, Alves D. Synthesis, photophysics and biomolecule interactive studies of new hybrid benzo-2,1,3-thiadiazoles. New J Chem (1987) 2020;44:2768–80. https://doi.org/10.1039/c9nj05932f.

[85] Gutierrez GD, Sazama GT, Wu T, Baldo MA, Swager TM. Red phosporescence from benzo[2,1,3]thiadiazoles at room temperature. J Org Chem 2016;81: 4789–96. https://doi.org/10.1021/acs.joc.6b00789.

[86] Mohanty ME, Madhu C, Reddy VL, Paramasivam M, Bangal PR, Rao VJ. Direct observation of the rise of delayed fluorescence in dithienylbenzothiadiazole and its role in the excited state dynamics of a donor-acceptor-donor molecule. Phys Chem Chem Phys 2017;19:9118–27. https://doi.org/10.1039/c7cp00261k.

[87] Jiang D, Chen S, Xue Z, Li Y, Liu H, Yang W, Li Y. Donor-acceptor molecules based on benzothiadiazole: synthesis, X-ray crystal structures, linear and third-order nonlinear optical properties. Dyes Pigments 2016;125:100–5. https://doi.org/10.1016/j.dyepig.2015.10.014.

[88] Isoppo VG, Rodembusch FS, Moro AV. Monosilylated 2,1,3-benzothiadiazole-based precursors. Molecular scaffolds for obtaining fluorescent organic-inorganic hybrid materials with tailored photophysical properties. Dyes Pigments 2023; 210:110978. https://doi.org/10.1016/j.dyepig.2022.110978.

[89] Liang A, Wang H, Chen Y, Zheng X, Cao T, Yang X, Cai P, Wang Z, Zhang X, Huang F. Benzoselenadiazole-based donor-acceptor small molecules: synthesis, aggregation-induced emission and electroluminescence. Dyes Pigments 2018; 149:399–406. https://doi.org/10.1016/j.dyepig.2017.10.20.

[90] Thomas KRP, Lin JT, Velusamy M, Tao YT, Chuen CH. Color tuning in benzo [1,2,5]thiadiazole-based small molecules by amino conjugation/deconjugation: bright red-light-emitting diodes. Adv Funct Mater 2004;14:83–90. https://doi.org/10.1002/adfm.200304486.

[91] Kawashima K, Osaka I, Takimiya K. Effect of chalcogen atom on the properties of naphthobischalcogenadiazole-based π-conjugated polymers. Chem Mater 2015; 27:6558–70. https://doi.org/10.1021/acs.chemmater.5b03124.

[92] Ye F, Chen W, Pan Y, Liu SH, Yin J. Benzobisthiadiazoles: from structure to function. Dyes Pigments 2019;171:107746. https://doi.org/10.1016/j.dyepig.2019.107746.

[93] Regis E, de O, Aguitar L, Tuzimoto P, Girotto E, Frizon TE, Dal Bo AG, Zapp E, Marra R, Gallardo H, Vieira A. Effect of heteroatom exchange (S/Se) in the mesomorphism and physical properties of benzochalcogenadiazole-based liquid crystals. Dyes Pigments 2018;157:109–16. https://doi.org/10.1016/j.dyepig.2018.04.049.

[94] Dorlus T, Wang J, Leszczynski J. Theoretical studies on the design of benzo[1,2-*c*:4,5-*c*']bis[1,2,5]selenadiazole acceptor-based dyes. Crystals (Basel) 2025;15:30. https://doi.org/10.103390/cryst15010030.

[95] Ishi-i T, Nakaya M, Umeki T, Matsumoto T, Lee JH, Yasuda T. Enchanced near-infrared phosphorescence found in a structurally similar host-guest system. J Mater Chem C 2024;12:19404–11. https://doi.org/10.1039/d4tc03441d.

[96] Marian CM. Spin-orbit coupling and intersystem crossing in molecules. WIREs Comput Mol Sci 2012;2:187–203. https://doi.org/10.1002/wcms.83.

[97] Fedorov DG, Koseki S, Schmidt MW, Gordon MS. Spin-orbit coupling in molecules: chemistry beyond the adiabatic approximation. Int Rev Phys Chem 2003;22:551–92. https://doi.org/10.1080/0144235032000101743.

[98] Hoover GC, Seferos DS. Photoactivity and optical applications of organic materials containing selenium and tellurium. Chem Sci 2019;10:9182–8. https://doi.org/10.1039/c9cs04279b.

[99] Langis-Barsetti S, Maris T, Wuest JD. Molecular organization of 2,1,3-benzothiadiazoles in the solid state. J Org Chem 2017;82:5034–45. https://doi.org/10.1021/acs.joc.6b02778.

[100] Bashirov DA, Sukhikh TS, Kuratieva NV, Chulanova EA, Yushina IY, Gritsan NP, Konchenko SN, Zibarev AV. Novel applications of functionalized 2,1,3-benzothiadiazoles for coordination chemistry and crystal engineering. RSC Adv 2014;4: 28309–16. https://doi.org/10.1039/c4ra03342f.

[101] Alfuth J, Czapik A, Zadykowicz B, Olszewska T. Hydrogen and chalcogen bonds in crystals of chalcogenadiazole carboxylic acids. CrystEngComm (Camb) 2024;26: 2918–27. d4ce00273c.

[102] Alfuth J, Zadykowicz B, Wicher B, Kazimierszuk K, Połoński T, Olszewska T. Cooperativity of halogen- and chalcogen-bonding in the self-assembly of 4-iodoethynyl- and 4,7-bis(iodoethynyl)benzo-2,1,3-chalcogenadiazoles: crystal structures, Hirshfeld analysis, and crystal lattice energy calculations. Cryst Growth Des 2022;22:1299–311. acs.cgd.1c01266.

[103] Axelsson MCF, Marchiori N, Huang P, Araujo CM, Tian H. Small organic molecules based on benzothiadiazole for electrocatalytic hydrogen production. J Am Chem Soc 2021;143:21229–33. https://doi.org/10.1021/jacs.1c10600.

[104] Pavlov DI, Yu X, Ryadun AV, Fedin VP, Potapov AS. Luminescent metal-organic framework with 2,1,3-benzothiadiazole units for highly sensitive gossipol sensing. Chemosensors 2023;11:52. https://doi.org/10.103390/chemosensors11010052.

[105] Li ZY, Zheng TF, Wen HR, Liu SJ. Recent progress of metal-organic framework materials with a benzothiadiazole unit for fluorescence sensing. CrystEngComm (Camb) 2025;27:713–28. https://doi.org/10.1039/d4ce01172d.

[106] Zhang Z, Huang J, Robertson LA, Assary RS, Shkrob IA, Zhang L. Elucidating factors controlling long-term stability of radical anions for negative charge storage in nonaqueous redox flow batteries. J Phys Chem C 2018;122:8116–27. https://doi.org/10.1021/acs.jpcc.8b01434.

[107] Huang J, Duan W, Zhang J, Shkrob IA, Assary RS, Pan B, Liao C, Zhang Z, Wei X, Zhang L. Substituted thiadiazoles as energy-rich analytes for nonaqueous redox flow cells. J Mater Chem A 2018;6:6251–4. https://doi.org/10.1039/c8ta01059e.

[108] Duan W, Huang J, Kowalski JA, Shkrob IA, Vijayakumar M, Walter E, Pan B, Yang Z, Milstein JD, Li B, Liao C, Zhang Z, Wang W, Liu J, Moore JS, Brushett FR, Zhang L, Wei X. Wine-dark sea in an organic flow battery: storing negative charge in 2,1,3-benzothiadiazole radicals leads to improved cyclability. ACS Energy Lett 2017;2:1156–61. acsenergylett.7b00261.

[109] Betowski LD, Enlow M, Raddick L, Aue DH. Calculation of electron affinities of polycyclic aromatic hydrocarbons and solvation energies of their radical anion. J Phys Chem A 2006;110:12927–46. https://doi.org/10.1021/jp065785v.

[110] Malloci G, Mulas G, Cappellini G, Fiorentini V, Porceddu I. Theoretical electron affinities of PAHs and electron absorption spectra of their mono-anions. Astron Astrophys 2005;432:585–94. https://doi.org/10.1051/0004-6361:20042246.

[111] Konstantinova LS, Knyazeva EA, Rakitin OA. Direct exchange of oxygen and selenium atoms in the 1,2,5-oxadiazoles and 1,2,5-selenadiazoles by action of sulfur monochloride. Molecules (Basel) 2015;20:14522–32. https://doi.org/10.3390/molecules200814522.

[112] Song S, Park S, Kwon S, Lee BH, Shim JY, Lee J, Park SH, Jin Y, Kim I, Lee K, Suh H. Synthesis and photovoltaic property of copolymers with phenanthrodiazole moiety. Sol Energy Mater Sol Cells 2012;105:229–36. https://doi.org/10.1026/j.solmat.2012.05.038.

[113] Lozeman JJA, Führer P, Olthuis W, Odijk M. Spectroelectrochemistry, the future of vizualizing electrode processes by hyphenating electrochemistry with spectroscopic techniques. Analyst 2020;145:2482–509. 10.1039.c9an02105a.

[114] Pylypenko A, Chulanova EA, Unger F, Keck J, Zaluzhnyy I, Dax I, Schwartzkopf M, Gerlach A, Hinderhofer A, Meixner AJ, Schreiber F. Thin films of conjugated chalcogenadiazole: growth, structure, and optical properties of substituted selenadiazoloquinoxaline. J Phys Chem C 2024;128:8104–13. https://doi.org/10.1021/acs.jpcc.4c01515.

[115] Neidlein R, Knecht D, Endres H. Synthesis and X-ray structure analysis of phenanthro[9,10-*c*]-1,2,5-telluradiazole. Z Naturforsch B Chem Sci 1987;42: 84–90. https://doi.org/10.1515/znb-1987-0116.

[116] Ishigaki Y, Shimomura K, Asai K, Shimajiri T, Akutagawa T, Fukushima T, Suzuki T. Chalcogen bond versus halogen bond: changing contributions in determining the crystal packing of dihalobenzochalcogenadiazoles. Bull Chem Soc Jpn 2022;95:522–31. https://doi.org/10.1246/bcsj.20220008.

[117] Bredas JL. Mind the gap. Mater Horiz 2014;1:17–9. https://doi.org/10.1039/c3mh00098b.

[118] Ottmers DM, Rase HF. Potassium graphites prepared by mixed-reaction techniques. Carbon 1966;4:125–7. https://doi.org/10.1016/0008-6223(66)90017-0.

[119] Sheldrick GM. Crystal structure refinement with *SHELXL*. Acta Crystallogr C 2015;71:3–8. https://doi.org/10.1107/s2053229614024218.

[120] Dolomanov OV, Bourhis LJ, Gildea RJ, Howard JAK, Puschmann H. *OLEX2*: a complete structure solution, refinement and analysis program. J Appl Crystallogr 2009;42:339–41. s0021889808042726.

[121] Bruker SAINT [software]. Bruker AXS, Madison, USA. 2009.

[122] Macrae CF, Edgington PR, McCabe P, Pidcock E, Shields GP, Taylor R, Towler M, van de Streek J. *Mercury*: vizualization and analysis of crystal structures. J Appl Crystallogr 2006;39:453–7. https://doi.org/10.1107/s002188980600731x.

[123] Bard A, Faulkner LR. Electrochemical methods. Fundamentals and applications. Wiley; 2001.

[124] Duling RD. Simulation of multiple isotropic spin-trap EPR spectra. J Magn Reson 1994;104:105–10. https://doi.org/10.1006/jmrb.1994.1062.

[125] Frisch MJ, Trucks GW, Schlegel HB, Scuseria GE, Robb MA, Cheeseman JR, Scalmani G, Barone V, Mennucci B, Petersson GA, Nakatsuji H, Caricato M, Li X, Hratchian HP, Izmaylov AF, Bloino J, Zheng G, Sonnenberg JL, Hada M, Ehara M, Toyota K, Fukuda R, Hasegawa J, Ishida M, Nakajima T, Honda Y, Kitao O, Nakai H, Vreven T, Montgomery JA, Peralta JE, Ogliaro F, Bearpark M, Heyd JJ, Brothers E, Kudin KN, Staroverov VN, Keith T, Kobayashi R, Normand J, Raghavachari K, Rendell A, Burant JC, Iyengar SS, Tomasi J, Cossi M, Rega N, Millam JM, Klene M, Knox JE, Cross JB, Bakken V, Adamo C, Jaramillo J, Gomperts R, Stratmann RE, Yazyev O, Austin AJ, Cammi R, Pomelli C, Ochterski JW, Martin RL, Morokuma K, Zakrzewski VG, Voth GA, Salvador P, Dannenberg JJ, Dapprich S, Daniels AD, Farkas O, Foresman JB, Ortiz JV, Cioslowski J, Fox DJ. Gaussian 09, revision D.01. Wallingford CT: Gaussian Inc.; 2013 [software].

[126] Laurent AD, Jacquemin D. TD-DFT benchmarks: a review. Quant Chem 2013;113: 2019–39. https://doi.org/10.1002/qua.24438.

[127] Bagryanskaya IY, Gatilov YV, Zibarev AV. Molecular structure of azachalcogenenes with aromatic substituents. J Struct Chem 1997;38:829–45. https://doi.org/10.1007/BF02763898.

[128] Tiekink ERT. Supramolecular aggregation patterns featuring Se···N secondary bonding intweractions in mono-nuclear compounds: a comparison with their congeners. Coord Chem Rev 2021;443:214031. https://doi.org/10.1016/j.ccr.2021.214031.

[129] Pomogaeva A, Cu FL, Imamura A, Aoki Y. Electronic structure and nonlinear optical properties of supramolecular associations of benzo-2,1,3-chalcogenadiazoles by the elongation method. Theor Chem Acta 2010;125: 453–60. https://doi.org/10.1007/s00214-009-0576-2.

[130] Cai Z, Zhang N, Awais MA, Filatov AS, Yu L. Synthesis of alternating donor-acceptor ladder-type molecules and investigation of their multiple charge-transfer pathways. Angew Chem Int Ed 2018;57:6442–8. https://doi.org/10.1002/anie.201713323.

[131] Alvarez S. A cartography of the van der Waals territories. Dalton Trans 2013;42: 8617–36. https://doi.org/10.1039/c3dt50599e.

[132] Luo J, Peng LM, Xue ZQ, Wu JL. Positive electron affinity of fullerenes: its effect and origin. J Chem Phys 2004;120:7998–8001. https://doi.org/10.1063/1.1691397.

[133] Mumyanov AV, Troshin PA. A review on fullerene derivatives with reduced electron affinity as acceptor materials for organic solar cells. Energies 2023;16: 1924. https://doi.org/10.3390/en16041924.

[134] Lin TS, Braun JR. The polarized electronic spectra and electric field spectra of benzo-diazoles. II. 2,1,3-Benzothiadiazole. Chem Phys 1978;28:379–86. https://doi.org/10.1016/0301-0104(78)80015-9.

[135] Lin TS, Braun JR. The polarized electronic spectra and electric field spectra of benzo-diazoles. I. 2,1,3-Benzoselenadiazole. Chem Phys 1977;26:403–11. https://doi.org/10.1016/0301-0104(77)85164-1.

[136] Sawicki E, Carr A. Structure of 2,1,3-benzoselenadiazole and its derivatives. I. Ultraviolet-visible absorption spectra. J Org Chem 1957;22:503–6. https://doi.org/10.1021/jo01356a007.

[137] Fabian J, Mayer R, Bleisch S. The absorbtion feature of conjugated compounds containing the NSN chromophore. Phosphorus Sulfur Relat Elem 1979;7:61–7. https://doi.org/10.1080/03086647808069924.

[138] Lin TS. EPR measurements of the phosphorescent state of 2,1,3-benzothiadiazole. Chem Phys Lett 1976;43:338–43. https://doi.org/10.1016/0009-2614(76)85315-8.

[139] Knyazeva EA, Rakitin OA. Influence of structural factors on the photovoltaic properties of dye-sensitized solar cells. Russ Chem Rev 2016;85:1146–83. https://doi.org/10.1070/RCR4649.

[140] Sukhikh TS, Khrisamov RM, Konchenko SN. Unexpectedly long lifetime of the excited state of benzothiadiazole derivative and its adduct with Lewis acids. Molecules (Basel) 2021;26:2030. https://doi.org/10.3390/molecules26072030.

[141] Loos PF, Jaquemin D. A mountaining strategy to excited states: highly accurate energies and benchmarks for bicyclic systems. J Phys Chem A 2021;125: 10174–88. https://doi.org/10.1021/acs.jpca.1c08524.

[142] Panwang Z. Why the lowest electronic excitations of rhodamines are overestimated by time-dependent density functional theory. Int J Quant Chem 2018;118:e25780. https://doi.org/10.1002/qua.25780.

[143] Shi H, Zou L, Huang K, Wang H, Sun C, Wang S, Ma H, He Y, Wang J, Yu H, Yao W, An Z, Zhao Q, Huang W. A highly efficient red metal-free organic phosphor for time-resolved luminescence imaging and photodynamic therapy. ACS Appl Mater Interfaces 2019;11:18103–10. https://doi.org/10.1021/acsami.9b01615.

[144] He G, Du L, Gong Y, Liu Y, Yu C, Wei C, Yuan WZ. Crystallization-induced red phosporescence and grinding-induced blue-shifted emission of benzobis(1,2,5-

thiadiazole)–thiophene conjugate. ACS Omega 2019;4:344–51. https://doi.org/10.1021/acsomega.8b02805.

[145] Zhu Z, Tian D, Gao P, Wang K, Li Y, Shu X, Zhu J, Zhao Q. Cell-dependent peptides transport noncovalently linked thermally delayed fluorescence nanoparticles for time-resolved luminescence imaging. J Am Chem Soc 2018;140:17484–91. https://doi.org/10.1021/jacs.8b08438.

[146] Noomnarm U, Clegg RM. Fluorescence lifetimes: fundamentals and interpretations. Photosynth Res 2009;101:181–94. https://doi.org/10.1007/s11120-009-9457-8.

[147] Berezin MY, Achilefu S. Fluorescence lifetime measurements and biological imagine. Chem Rev 2010;110:2641–84. https://doi.org/10.1021/cr9003432.

[148] Sherman EO, Lambert SM, Pilgram K. Polarography of some 2,1,3-benzothiadiazoles, benzofurazans, 2,1,3-benzoselenadiazoles, and 3,4-disubstituted and fused 1,2,5-thiadiazoles. J. Heterocyclic. Chem 1974;11:763–9. https://doi.org/10.1002/jhet.5570110519.

[149] Odintsov DS, Shundrina IK, Gorbunov DE, Gritsan NP, Beckmann J, Shundrin LA. Spectroelectrochemical study of the reduction of 2-methyl-9*H*-thioxantene-9-one and its *S,S*-dioxide and electronic absorption spectra of their molecular ions. Phys Chem Chem Phys 2021;23:26940–7. https://doi.org/10.1039/d1cp04464h.

[150] Konchenko SN, Gritsan NP, Lonchakov AV, Radius U, Zibarev AV. Isolation of the 2,1,3-benzothiadiazolyl radical anion: X-ray structure and properties of a [K(THF)][$C_6H_4N_2S$] salt. Mendeleev Commun 2009;19:7–9. https://doi.org/10.1016/j.mencom.2009.01.003.

[151] Semenov NA, Radiush EA, Chulanova EA, Slawin AMZ, Woollins JD, Kadilenko EM, Bagryanskaya IY, Irtegova IG, Bogomyakov AS, Shundrin LA, Gritsan NP, Zibarev AV. Design, synthesis and isolation of a new 1,2,5-selenadiazolidyl and structural and magnetic characterization of its alkali-metal salts. New J Chem (1987) 2019;43:16331–7. https://doi.org/10.1039/c9nj04069b.

[152] Gritsan NP, Lonchakov AV, Lork E, Mews R, Pritchina EA, Zibarev AV. Diamagnetic π-dimers of the [1,2,5]thiadiazolo[3,4-*c*][1,2,5]thiadiazolidyl radical anion in the crystalline state: preparation and X-ray crystal structure of a $[(Me_2N)_2CC(NMe_2)_2]^{2+}[(C_2N_4S_2)_2]^{2-}$ salt. Eur J Inorg Chem 2007;2007:1994–8. https://doi.org/10.1002/ejic.200701136.

[153] Chulanova EA, Pritchina EA, Malaspina LA, Grabowsky S, Mostaghimi F, Beckmann J, Bagryanskaya IY, Shakhova MV, Konstantinova LS, Rakitin OA, Gritsan NP, Zibarev AV. New charge-transfer complexes with 1,2,5-thiadiazoles as both electron acceptors and donors featuring an unprecedented addition reaction. Chem Eur J 2017;23:852–64. https://doi.org/10.1002/chem.201604121.

[154] Pushkarevsky NA, Lonchakov AV, Semenov NA, Lork E, Buravov LI, Konstantinova LS, Silber GT, Robertson N, Gritsan NP, Rakitin OA, Woollins JD, Yagubskii EB, Beckmann J, Zibarev AV. First charge-transfer complexes between tetrathiafulvalene and 1,2,5-chalcogenadiazole derivatives: design, synthesis, crystal structures, electronic and electrical properties. Synth Met 2012;162:2267–76. https://doi.org/10.1016/j.synthmet.2012.10.026.

[155] Chulanova EA, Radiush EA, Balmohammadi Y, Beckmann J, Grabowsky S, Zibarev AV. New charge-transfer complexes of 1,2,5-chalcogenadiazoles with tetrathiafulvalenes. CrystEngComm (Camb) 2023;25:391–402. https://doi.org/10.1039/d2ce01385a.

[156] Odintsov DS, Gismatulin AA, Shundrina IK, Buktoyarova AD, Os'kina IA, Beckmann J, Azarov IA, Dementeva EV, Shundrin LA. Gritsenko VA Methyl methacrylate copolymer with pendant thioxanthenone groups as active layer for resistive memory devices. ChemPhysChem 2024;25:e202400266. https://doi.org/10.1002/cphc.202400266.

[157] Shundrina IK, Os'kina IA, Odintsov DS, Gismatulin AA, Azarov IA, Shundrin LA, Gritsenko VA. Octafluorobiphenyl-4,4'-diyl 9-oxothioxanthene-1,4-diyl polyether – a promising material for organic film based memristors: synthesis, memristive effect and charge transport mechanism. Mendeleev Commun 2024;34:667–9. https://doi.org/10.1016/j.mencom.2024.09.013.

[158] Gismatulin AA, Odintsov DS, Shundrina IK, Os'kina IA, Azarov IA, Shundrin LA, Gritsenko VA. Charge transport mechanism and trap origin in methyl methacrylate copolymer with thioxanthenone side groups. Chem Phys Lett 2024;840:141140. https://doi.org/10.1016/j.cplett.2024.141140.

[159] Kang J, Shin DJ, Lee JY. Recent advances in narrow emission bandwidth materials for applications in organic light-emitting diodes. Adv Opt Mater 2025;23:2402653. https://doi.org/10.1002/adom.202402653.

[160] Dubinets NO, Sosorev AY. Fluorescent properties of novel multiresonant indolocarbazole derivatives for deep-blue OLEDS from multiscale computer modeling. Molecules (Basel) 2025;30:255. https://doi.org/10.3390/molecules30020255.

[161] Linnemannstöns M, Schwabendissen J, Neumann B, Stammler HG, Berger RJF, Mitzel NW. Aryl-aryl interactions in (Aryl-perhalogenated) 1,2-diaryldisilanes. Chem Eur J 2020;26:2169–73. https://doi.org/10.1002/chem.201905727.

[162] Linnemannstöns M, Schwabendissen J, Schultz AA, Neumann B, Stammler HG, Berger RJF, Mitzel NW. London dispersion-driven hetero-aryl-aryl interactions in 1,2-diaryldisilanes. Chem Commun 2019;56:2252–5. https://doi.org/10.1039/c9cc09851h.

[163] Blomeyer S, Linnemannstöns M, Niessen JH, Paulus J, Neumann B, Stammler HG, Mitzel NW. Intramolecular π-π interactions in flexibly linked partially fluorinated bisarenes in the gas phase. Angew Chem Int Ed 2017;56:13259–63. https://doi.org/10.1002/anie.201707716.

[164] Lork E, Mews R, Shakirov MM, Watson PG, Zibarev AV. Reactions of arylthiazylamides with internal and external fluoro electrophiles – formation of products with unusual structures. Eur J Inorg Chem 2001;2001:2123–34. https://doi.org/10.1002/1099-0682(200108)2001:8<2123::AID-EJIC2123>3.0.CO;2-G.

[165] Bacchi S, Beneglia M, Cozzi F, Demartin F, Filipini G, Gavezzoti A. X-ray diffraction and theoretical studies for the quantitative assessment of intermolecular arene-perfluoroarene stacking interactions. Chem Eur J 2006;12:3538–46. https://doi.org/10.1002/chem.200501248.

[166] Pluhǎkova K, Jurečka P, Hobza P. Stabilization energy of $C_6H_6\cdots C_6X_6$ (X = F, Cl, Br, I, CN) complexes: complete basis set limit calculations at MP2 and CCSD(T) levels. Phys Chem Chem Phys 2007;9:755–60. https://doi.org/10.1039/b615318f.

[167] Berger R, Resnati G, Matrangolo P, Hulliger J. Organic fluorine compounds: a great opportunity for enhanced materials properties. Chem Soc Rev 2011;40:3496–508. https://doi.org/10.1039/c0cs00221f.

[168] Tang ML, Bao Z. Halogenated materials as organic semiconductors. Chem Mater 2011;23:446–55. https://doi.org/10.1021/cm102182x.

[169] Babudri F, Farinola GM, Naso F, Ragni R. Fluorinated organic materials for electronic and optoelectronic applications: the role of fluorine atom. Chem Commun 2007:1003–22. https://doi.org/10.1039/b611336b.

[170] Reichenbächer K, Süss HI, Hulliger J. Fluorine in crystal engineering – the little atom that could. Chem Soc Rev 2005;34:22–30. https://doi.org/10.1039/b406892k.

[171] Ocheje MU, Comí M, Yang R, Chen Z, Liu Y, Yousefi N, Al-Hashimi M, Rondeau-Gagnè S. Molecular engineering of benzothiadiazole-based polymers: balancing charge transport and stratchability in organic field-effect transistors. J Mater Chem C 2022;10:4236–46. https://doi.org/10.1039/d1tc06103h.

[172] Wang Y, Tan ATR, Mori T, Michinobu T. Inversion of charge carrier polarity and boosting the mobility of organic semiconducting polymers based on benzobisthiadiazole derivatives by fluorination. J Mater Chem C 2018;6:3593–603. https://doi.org/10.1039/c7tc04993e.

[173] Li M, Li Z, Song G, Jiang C, Chen X, Wang J, Yang Y, Wan X, Li C, Chan Y. π-Extended chlorinated non-fullrerene acceptors for achieving high-performance organic solar cells. J Mater Chem C 2023;11:1155–64. https://doi.org/10.1039/d2tc04311d.

[174] Radiush EA, Sukhikh TS. Unpublished results.

[175] Vasilieva NV, Irtegova IG, Gritsan NP, Lonchakov AV, Makarov AY, Shundrin LA, Zibarev AV. Redox properties and radical anions of fluorinated 2,1,3-benzothia(selena)diazoles and related compounds. J Phys Org Chem 2010;23:536–43. https://doi.org/10.1002/poc.1673.